omy [14–17]. However, little information is available on the alterations in the expression of renal organic ion transporters during the recovery from renal impairment. On one hand, renal functions were decreased in hyperuricemic rats induced by the administration of a chow containing uric acid and oxonic acid, an inhibitor of uric acid metabolism [18]. After administration of the chow was discontinued, renal functions such as the fractional reabsorption of sodium and phosphate were improved, although the urine concentrating ability, calcium reabsorption and the capacity to excrete ammonium remained impaired [18]. Therefore, renal functions including renal organic ion transport might change at different rates during recovery from hyperuricemia in rats.

In the present study, we examined the alteration of organic ion transport activity and the expression of organic ion transporters including rOAT1, rOAT3 and rOCT2 in the kidney during recovery from hyperuricemia in rats.

2. Materials and methods

2.1. Materials

D-[1-^{3}H(*N*)]-mannitol (973 GBq/mmol) and *p*-[glycyl-1-^{14}C]-aminohippuric acid (1.9 GBq/mmol) were obtained from Perkin-Elmer™ Life Sciences. [1-^{14}C] Tetraethylammonium bromide (2.04 GBq/mmol) was obtained from American Radiolabeled Chemicals. Oxonic acid and uric acid were purchased from Aldrich and Wako Pure Chemical Industries, respectively. All other chemicals used were of the highest purity available.

2.2. Animals

The animal experiments were performed in accordance with the Guidelines for Animal Experiments of Kyoto University. The experimental protocol was approved by the Animal Research Committee, Graduate School of Medicine, Kyoto University. Male Wistar rats weighing 190–235 g were fed ground rat chow and water freely for 10–24 days. Hyperuricemia was induced with ground standard rat chow containing 2.5% uric acid and 5% oxonic acid for 10 days as described in our previous report (0-day recovery group) [13]. During recovery from hyperuricemia, the rats were fed standard rat chow for 4, 7 or 14 days (4, 7 or 14-day recovery group).

2.3. Biochemical tests

The concentration of blood urea nitrogen (BUN) and creatinine in plasma and urine were measured by the urease–indophenol method and Jaffé method using kits obtained from Wako Pure Chemical Industries, respectively. Plasma uric acid concentration was determined by high performance liquid chromatography as described in the previous report [13]. Plasma concentration of testosterone was measured with an enzyme immunoassay kit (Cayman Chemical Company).

2.4. Histological analyses

Kidneys of rats during recovery from hyperuricemia were removed and immediately fixed for 1 day at room temperature in carnoy fixative (ethanol:chloroform:acetic acid = 6:3:1) and preserved in 70% ethanol. Conventional histological sections were stained with periodic acid-Schiff reagent [8].

2.5. Uptake of PAH and TEA into renal slices

Renal slices were prepared with a Stadie–Riggs microtome and the uptake of [^{14}C]PAH (5 μM, 0.93 kBq/mL) or [^{14}C]TEA (5 μM, 1.03 kBq/mL) were measured as previously described [13]. [^{3}H]Mannitol (5 μM, 22.8 kBq/mL) was used to calculate the extracellular trapping and nonspecific uptake of [^{14}C]PAH and [^{14}C]TEA as well as to evaluate the viability of slices.

2.6. Western blot analyses

Preparation of crude membrane fractions and Western blot analyses were performed as previously reported [13].

2.7. Northern blot analyses

Total RNA was extracted from the kidney using TRIZOL™ reagent (Invitrogen Co.). Then, Northern blot analyses were performed as previously described [13].

2.8. Statistical analyses

The statistical significance of differences between mean values was calculated using the non-paired *t*-test, or by the one-way analysis of variance with the Scheffé test for post hoc analysis. *P*-values of <0.05 were considered significant.

3. Results

Several physiological and biochemical parameters were measured during the recovery period of hyperuricemia in rats (Fig. 1). The body weight gradually increased during recovery for 14 days. Plasma uric acid returned to the normal level during the initial 4 days of recovery. Improvement of BUN, plasma creatinine and creatinine clearance during the initial 4 days suggested that renal functions have been recovered quickly. In contrast, urine volume returned to normal more slowly than the above parameters.

Histological analyses of the kidney were performed and shown in Fig. 2. The tubular lumen was dilated in a diffuse

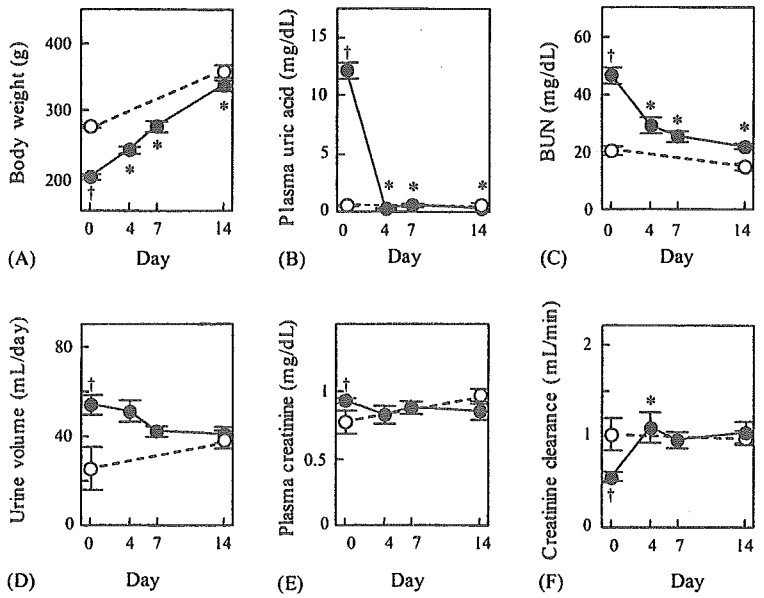

Fig. 1. Physiological and biochemical parameters during recovery from hyperuricemia. At 4, 7 and 14 days recovery from hyperuricemia, body weight (A), plasma uric acid (B), BUN (C), urine volume (D), plasma creatinine (E) and creatinine clearance (F) were measured (●). Open circles represent the values of normal rats. Each point represents the mean ± S.E. of 5–13 rats. $^{\dagger}P < 0.05$, vs. normal rats. $^{*}P < 0.05$, vs. hyperuricemic rats on day 0.

area filled with detached tubular epithelial cells and was infiltrated by mono- and poly-nuclear cells in hyperuricemic rat kidney (0-day recovery group) as previously reported [13]. Moreover, inflammatory cells also infiltrated into the interstitium and in tubules [13]. This tubulointerstitial pathology was observed in the diffuse area on day 4, and visible in the focal area on day 7, which was almost disappeared on day 14 (Fig. 2).

We then evaluated basolateral organic anion and cation transport activity by the uptake of PAH and TEA into renal slices (Fig. 3). The PAH and TEA uptake into renal slices in the 0-day recovery group were much lower than those in normal rats. In the 4-days recovery group, PAH and TEA uptake were significantly increased compared with those in 0-day recovery group. The PAH and TEA uptake in the 14-days recovery groups achieved similar uptake activity to those in control group at 30 or 60 min.

The expression of rOAT1, rOAT3 and rOCT2 protein during the recovery period of hyperuricemic rats was examined by Western blot analyses (Fig. 4). The expression of these transporters of 0-day recovery group was significantly decreased in hyperuricemic rats compared with normal rats, and the expression levels of rOAT1 and rOAT3 in 7- and 14-days recovery group significantly increased compared with those in 0-day recovery group. The expression of rOCT2 protein gradually increased until 14-days of recovery.

The mRNA expression of rOAT1 and rOCT2 during recovery from hyperuricemia was analyzed by Northern blot analyses (Fig. 5). The mRNA expression of both transporters in the 0-day recovery group was much lower than that in normal rats, and the rOAT1 mRNA expression significantly increased in the 7- and 14-days recovery group compared with 0-day recovery group. Recovery of rOCT2 mRNA expression was significant on day 14. Moreover, the expression of rOAT1 and rOCT2 protein was significantly correlated with that of mRNA, respectively (rOAT1, $r^2 = 0.66$, $P < 0.05$; rOCT2, $r^2 = 0.45$, $P < 0.05$).

We investigated the correlation between basolateral PAH and TEA transport and the protein level of rOAT1, rOAT3 and rOCT2 (Fig. 6). Initial PAH transport at 15 min across basolateral membrane showed a high correlation with the protein level of rOAT1 ($r^2 = 0.80$, $P < 0.05$), but not with that of rOAT3 ($r^2 = 0.34$, $P = 0.35$). On one hand, basolateral TEA transport showed a high correlation with the protein level of rOCT2 ($r^2 = 0.91$, $P < 0.05$).

Finally, we measured plasma concentration of testosterone, which was the dominant factor mediating sex-related difference in the expression of rOCT2 [19]. Plasma testosterone concentration was decreased in the 0-day recovery group (control, 3.23 ± 0.59 ng/mL; 0 day, 1.08 ± 0.10 ng/mL; mean ± S.E., $n = 6$) and was gradually increased during the recovery period of hyperuricemia (4 days, 1.68 ± 0.45 ng/mL; 7 days, 3.61 ± 0.24 ng/mL; 14 days, 4.51 ± 1.26 ng/mL; mean ± S.E., $n = 6$). However, plasma testosterone levels and the expression of rOCT2 protein did not show a significant linear correlation (Fig. 7, $r^2 = 0.14$, $P = 0.14$).

4. Discussion

Hyperuricemia is often the first clinical manifestation of gout and accompanies renal failure. Recently, serum uric

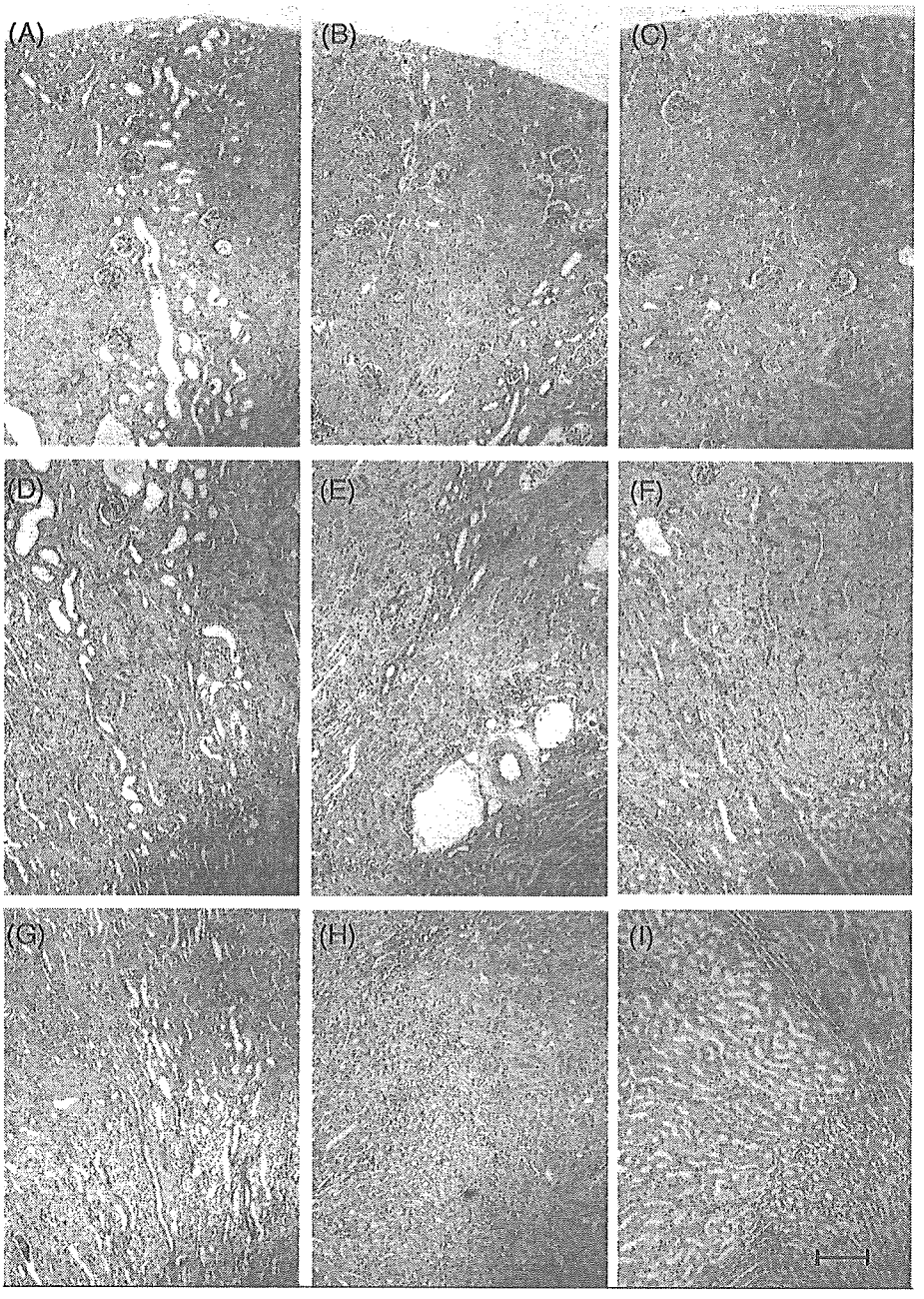

Fig. 2. Periodic acid-Schiff staining of cortex (A–C), outer medulla (D–F) and inner medulla (G–I) in the serial picture from each typical rat kidney at 4—(A, D and G), 7—(B, E and H) and 14—(C, F and I) days recovery from hyperuricemia; bar = 100 μm.

acid was found to be an independent risk factor for development of renal insufficiency in a study of 6403 subjects [20]. Mazaali et al. reported that crystal-independent mechanism, mediated in part by activation of the renin-angiotensin system and downregulation of NO synthase expression, contributed to renal injury in hyperuricemia [21]. Actually, we did not observe urate crystals in any part of kidneys in our experiments (Fig. 2). We previously reported that plasma creatinine and BUN levels increased, and that basolateral organic ion transport activity decreased, accompanied with specifically decreased expression of rOAT1, rOAT3 and rOCT2 in the kidney of hyperuricemic rats [13]. In this study, we investigated renal organic ion transport activity and the expression of rOAT1, rOAT3 and rOCT2 in kidney during recovery from hyperuricemia.

During the initial 4 days, BUN, plasma creatinine and creatinine clearance were restored significantly (Fig. 1), suggesting that renal functions recovered quickly. On the other hand, the recovery of tubulointerstitial injury was varied in sites of the kidney, probably because of the different severity of damage as shown in Fig. 2. Organic anion and cation transport activity across basolateral membranes and the expression of organic ion transporters, rOAT1, rOAT3 and rOCT2 in the kidney also gradually improved (Figs. 3 and 4). Interestingly, basolateral PAH

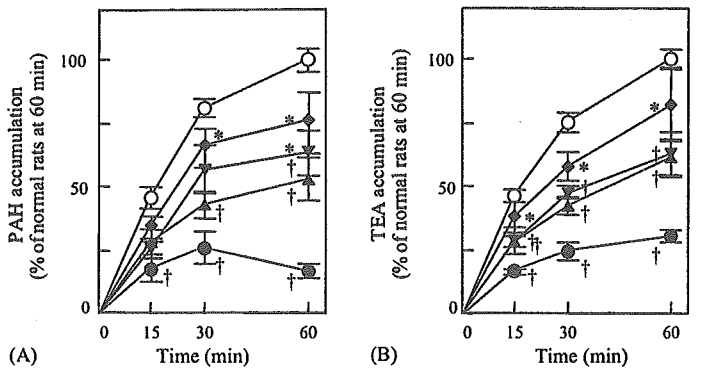

Fig. 3. Accumulation of PAH (A) and TEA (B) into renal slices during the recovery from hyperuricemia. Renal slices from normal (○) and hyperuricemic rats at 0: ●, 4: ▲, 7: ▼ and 14: ◆ days of recovery were incubated at 25 °C in incubation buffer containing 5 μM [^{14}C]PAH or 5 μM [^{14}C]TEA for the periods indicated. D-[^{3}H]Mannitol was used to estimate the extracellular trapping and non-specific uptake of [^{14}C]PAH and [^{14}C]TEA. Each point represents the mean ± S.E. for 5–8 slices from different rats. $^{\dagger}P < 0.05$, vs. normal rats. $^{*}P < 0.05$, vs. hyperuricemic rats on day 0.

transport showed a higher correlation with the protein level of rOAT1 than that of rOAT3 (Fig. 6), demonstrating that rOAT1 was a dominant transporter mediating the basolateral uptake of PAH. Basolateral TEA transport showed a high correlation with the protein level of rOCT2 (Fig. 6). As far as we know, this is the first report demonstrating the restoration of renal organic ion transporters (slc22a) during recovery from renal impairment, accompanying the change of basolateral uptake of PAH and TEA in the kidney.

The expression of rOCT2 is regulated by testosterone [19]. In contrast to rOCT2, renal expression of rOAT1 and rOCT1 was not changed between male and female, suggesting little or no contribution of testosterone in the regulation of renal rOAT1 and rOCT1 [22]. In addition, both plasma testosterone levels and the expression levels of rOCT2 decreased in 5/6 nephrectomized rats, where the expression levels of rOCT2 were restored by the administration of physiological concentrations of testosterone [17]. In clinical cases, a lower serum testosterone level was reported to be associated with chronic renal failure [23,24]. In the present study, both rOCT2 expression and plasma testosterone concentration decreased in hyperuricemia, and were restored to normal during recovery from hyperuricemia. However, the correlation between rOCT2 expression and plasma testosterone concentration was not significant. These results suggested that the decreased plasma testosterone level was one of the determinants of rOCT2 expression in hyperuricemic rats.

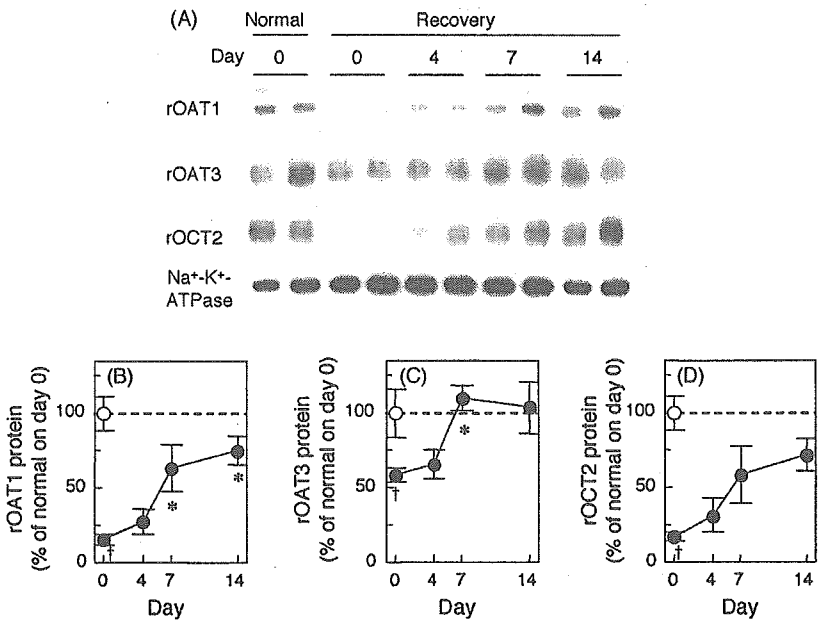

Fig. 4. Western blot analyses of rOAT1, rOAT3 and rOCT2 in crude membrane fractions from the kidneys during recovery from hyperuricemia. Crude membrane fractions from the kidneys of normal and hyperuricemic rats at 0, 4, 7 and 14 days of recovery were separated by SDS-PAGE. rOAT1, rOAT3, rOCT2 and Na^+-K^+-ATPase α-1 subunit were identified with each antibody. The results in a typical experiment are shown in panel (A). The ratio of rOAT1 (B), rOAT3 (C) and rOCT2 (D) density to Na^+-K^+-ATPase α-1 subunit density. Each point represents the mean ± S.E. for three normal (○) and four hyperuricemic (●) rats from two experiments. $^{\dagger}P < 0.05$, vs. normal rats. $^{*}P < 0.05$, vs. hyperuricemic rats on day 0.

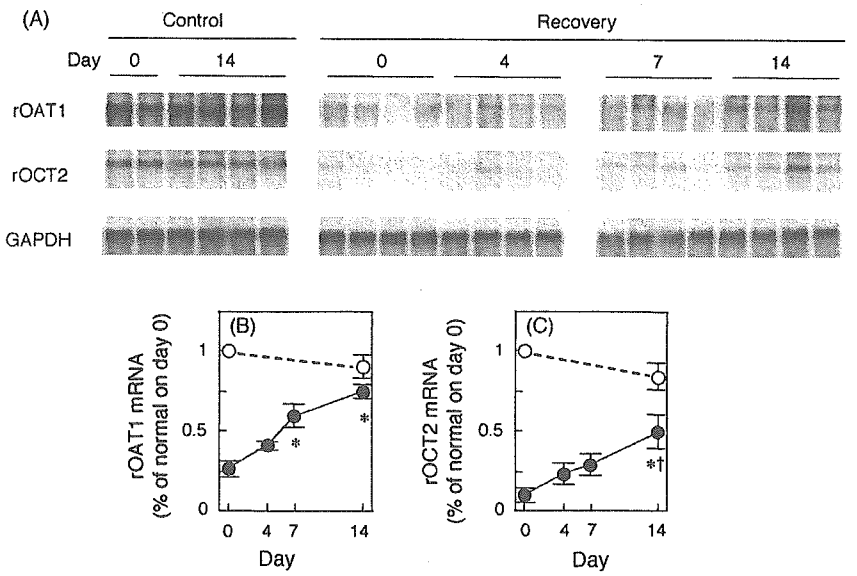

Fig. 5. Northern blot analyses of rOAT1 and rOCT2 during recovery from hyperuricemia. Total RNA (5 μg) from the kidneys of normal and hyperuricemic rats at 0, 4, 7 and 14 days of recovery was hybridized with rOAT1, rOCT2 and GAPDH cDNA probes under high stringency. The results in a typical experiment are shown in panel (A). Densitometry of rOAT1 (B) and rOCT2 (C) mRNAs was corrected for loading with GAPDH mRNA. Each point represents the mean ± S.E. for two to four normal (○) and four hyperuricemic (●) rats. $^{\dagger}P < 0.05$, vs. normal rats. $^{*}P < 0.05$, vs. hyperuricemic rats on day 0.

The dosage regimen of various drugs for patients with renal insufficiency is generally determined according to the value of creatinine clearance. However, renal excretion of ionic drugs into urine is mediated not only by glomerular filtration but also by tubular secretion via organic anion and cation transporters. Actually, the dosage schedule based on creatinine clearance was demonstrated to be inadequate for ampicillin and cephalexin dosing in some patients with renal insufficiency [25]. Recently, we reported that the elimination rate of cefazolin, which is a substrate of hOAT3, was significantly correlated with the levels of hOAT3 mRNA in humans [26]. In the present study, basolateral uptake of PAH and TEA in the kidney was significantly correlated with the expression of rOAT1 and

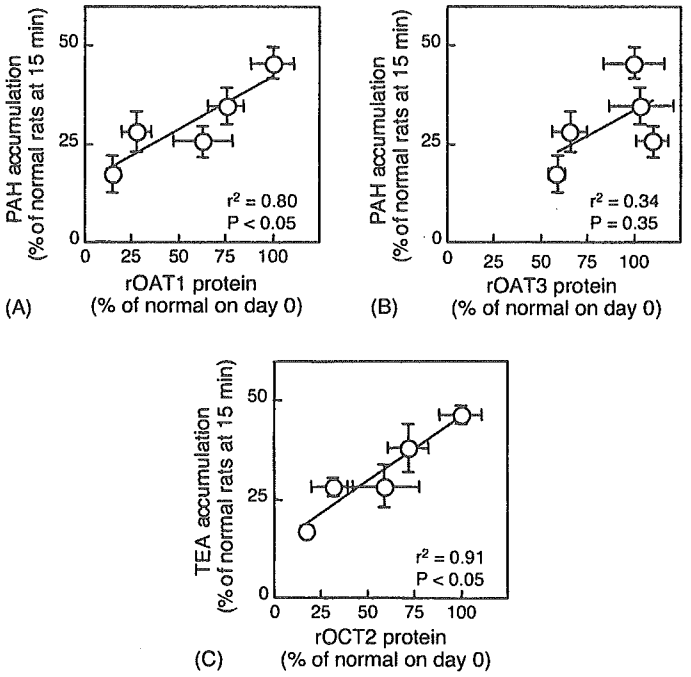

Fig. 6. Correlation between protein levels of rOAT1 (A), rOAT3 (B) and rOCT2 (C) and initial uptake activity of PAH (A and B) and TEA (C) by the renal slices during recovery from hyperuricemia. The linear regression was obtained with the mean values of rOAT1, rOAT3 and rOCT2 at protein levels and initial uptake activity of PAH and TEA. Each point represents the mean ± S.E. obtained in Figs. 3 and 4.

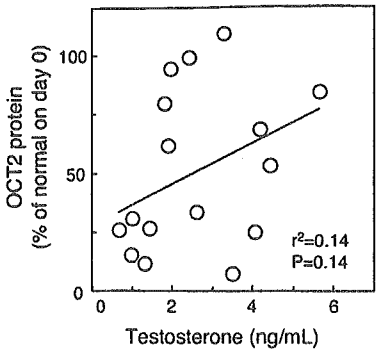

Fig. 7. Correlation between plasma testosterone and rOCT2 protein levels in the kidney during recovery from hyperuricemia. The linear regression was obtained with the plasma concentration of testosterone and rOCT2 protein levels of 17 rats during recovery from hyperuricemia.

rOCT2, respectively. Moreover, the recovery rate of rOAT1, rOAT3 and rOCT2 expression was slower than that of creatinine clearance. Based on these findings, dosage regiments according to the activity of organic anion and cation transport in addition to creatinine clearance should be helpful for precise dosage regimen in the patients with renal dysfunctions.

In conclusion, renal expression of organic ion transporters, rOAT1, rOAT3 and rOCT2, was reversibly regulated by hyperuricemia, accompanying the change of organic ion transport. Although further clinical investigations on the expression levels of drug transporters in several disease states are needed, the expression profiles of drug transporters may be useful information for understanding the alteration of renal drug secretion.

Acknowledgments

This work was supported in part by a Grant-in-Aid for Scientific Research from the Ministry of Education, Culture, Sports, Science and Technology of Japan.

References

[1] Pritchard JB, Miller DS. Mechanisms mediating renal secretion of organic anions and cations. Physiol Rev 1993;73:765–96.
[2] Inui K, Masuda S, Saito H. Cellular and molecular aspects of drug transport in the kidney. Kidney Int 2000;58:944–58.
[3] Sekine T, Watanabe N, Hosoyamada M, Kanai Y, Endou H. Expression cloning and characterization of a novel multispecific organic anion transporter. J Biol Chem 1997;272:18526–9.
[4] Sweet DH, Wolff NA, Pritchard JB. Expression cloning and characterization of ROAT1. The basolateral organic anion transporter in rat kidney. J Biol Chem 1997;272:30088–95.
[5] Cha SH, Sekine T, Fukushima J, Kanai Y, Kobayashi Y, Goya T, et al. Identification and characterization of human organic anion transporter 3 expressing predominantly in the kidney. Mol Pharmacol 2001; 59:1277–86.
[6] Sekine T, Cha SH, Endou H. The multispecific organic anion transporter (OAT) family. Pflügers Arch 2000;440:337–50.
[7] Uwai Y, Okuda M, Takami K, Hashimoto Y, Inui K. Functional characterization of the rat multispecific organic anion transporter OAT1 mediating basolateral uptake of anionic drugs in the kidney. FEBS Lett 1998;438:321–4.
[8] Motohashi H, Sakurai Y, Saito H, Masuda S, Urakami Y, Goto M, et al. Gene expression levels and immunolocalization of organic ion transporters in the human kidney. J Am Soc Nephrol 2003;13:866–74.
[9] Gründemann D, Gorboulev V, Gambaryan S, Veyhl M, Koepsell H. Drug excretion mediated by a new prototype of polyspecific transporter. Nature 1994;372:549–52.
[10] Okuda M, Saito H, Urakami Y, Takano M, Inui K. cDNA cloning and functional expression of a novel rat kidney organic cation transporter, OCT2. Biochem Biophys Res Commun 1996;224:500–7.
[11] Koepsell H, Gorboulev V, Arndt P. Molecular pharmacology of organic cation transporters in kidney. J Membr Biol 1999;167:103–17.
[12] Urakami Y, Okuda M, Masuda S, Akazawa M, Saito H, Inui K. Distinct characteristics of organic cation transporters, OCT1 and OCT2, in the basolateral membrane of renal tubules. Pharm Res 2001;18:1528–34.
[13] Habu Y, Yano I, Takeuchi A, Saito H, Okuda M, Fukatsu A, et al. Decreased activity of basolateral organic ion transports in hyperuricemic rat kidney: roles of organic ion transporters, rOAT1, rOAT3 and rOCT2. Biochem Pharmacol 2003;66:1107–14.
[14] Huang Q, Dunn II RT, Jayadev S, DiSorbo O, Pack FD, Farr SB, et al. Assessment of cisplatin-induced nephrotoxicity by microarray technology. Toxicol Sci 2001;63:196–207.
[15] Demeule M, Brossard M, Béliveau R. Cisplatin induces renal expression of P-glycoprotein and canalicular multispecific organic anion transporter. Am J Physiol Renal Physiol 1999;277:F832–40.
[16] Laouari D, Yang R, Veau C, Blanke I, Friedlander G. Two apical multidrug transporters, P-gp and MRP2, are differently altered in chronic renal failure. Am J Physiol Renal Physiol 2001;280:F636–45.
[17] Ji L, Masuda S, Saito H, Inui K. Down-regulation of rat organic cation transporter rOCT2 by 5/6 nephrectomy. Kidney Int 2002;62:514–24.
[18] Brown EA, Kliger AS, Hayslett JP, Finkelstein FO. Renal function in rats with acute medullary injury. Nephron 1980;26:64–8.
[19] Urakami Y, Okuda M, Saito H, Inui K. Hormonal regulation of organic cation transporter OCT2 expression in rat kidney. FEBS Lett 2000;473:173–6.
[20] Iseki K, Oshiro S, Tozawa M, Iseki C, Ikemiya Y, Takishita S. Significance of hyperuricemia on the early detection of renal failure in a cohort of screened subjects. Hypertens Res 2001;24:691–7.
[21] Mazaali M, Hughes J, Kim Y-G, Jefferson JA, Kang D-H, Godon KL, et al. Elevated uric acid increases blood pressure in the rat by a novel crystal-independent mechanism. Hypertension 2001;38: 1101–1106.
[22] Urakami Y, Nakamura N, Takahashi K, Okuda M, Saito H, Hashimoto Y, et al. Gender differences in expression of organic cation transporter OCT2 in rat kidney. FEBS Lett 1999;461:339–42.
[23] Joven J, Villabona C, Rubies-Prat J, Espinel E, Galard R. Hormonal profile and serum zinc levels in uraemic men with gonadal dysfunction undergoing haemodialysis. Clin Chim Acta 1985;148:239–45.
[24] Mitchell R, Bauerfeld C, Schaefer F, Scharer K, Rovertson WR. Less acidic forms of luteinizing hormone are associated with lower testosterone secretion in men on haemodialysis treatment. Clin Endocrinol 1994;41:65–73.
[25] Hori R, Okumura K, Kamiya A, Nihira H, Nakano H. Ampicillin and cephalexin in renal insufficiency. Clin Pharmacol Ther 1983;34: 792–8.
[26] Sakurai Y, Motohashi H, Ueo H, Masuda S, Saito H, Okuda M, et al. Expression levels of renal organic anion transporters (OATs) and their correlation with anionic drug excretion in patients with renal diseases. Pharm Res 2004;21:61–7.

Am J Physiol Gastrointest Liver Physiol 288: G664–G670, 2005.
First published November 4, 2004; doi:10.1152/ajpgi.00270.2004.

Increased protein level of PEPT1 intestinal H^+-peptide cotransporter upregulates absorption of glycylsarcosine and ceftibuten in 5/6 nephrectomized rats

Yuriko Shimizu, Satohiro Masuda, Kumiko Nishihara, Lin Ji, Masahiro Okuda, and Ken-ichi Inui
Department of Pharmacy, Kyoto University Hospital, Faculty of Medicine, Kyoto University, Sakyo-ku, Kyoto, Japan

Submitted 22 June 2004; accepted in final form 3 November 2004

Shimizu, Yuriko, Satohiro Masuda, Kumiko Nishihara, Lin Ji, Masahiro Okuda, and Ken-ichi Inui. Increased protein level of PEPT1 intestinal H^+-peptide cotransporter upregulates absorption of glycylsarcosine and ceftibuten in 5/6 nephrectomized rats. *Am J Physiol Gastrointest Liver Physiol* 288: G664–G670, 2005. First published November 4, 2004; doi:10.1152/ajpgi.00270.2004.—In chronic renal failure (CRF), dietary protein is one of the factors that deteriorates residual renal functions. Numerous studies have indicated that the products of protein digestion are mainly absorbed as small peptides. However, how small peptides are absorbed in CRF remains poorly understood. H^+-coupled peptide transporter (PEPT1/*SLC15A1*) plays an important role in the absorption of small peptides and peptide-like drugs in the small intestine. Because dietary protein intake is one of the risk factors for renal failure, the alteration of intestinal PEPT1 might have implications in the progression of renal disease as well as the pharmacokinetics of peptide-like drugs. In this study, we examined the alteration of intestinal PEPT1 in 5/6 nephrectomized (5/6 NR) rats, extensively used as a model of chronic renal failure. Absorption of [^{14}C]glycylsarcosine and ceftibuten was significantly increased in 5/6 NR rats compared with sham-operated rats, without a change in intestinal protease activity. Western blot analysis indicated that the amount of intestinal PEPT1 protein in 5/6 NR rats was increased mainly at the upper region. On the other hand, the amount of intestinal PEPT1 mRNA was not significantly different from that of sham-operated rats. These findings indicate that the increase in absorption of small peptides and peptide-like drugs, caused by the upregulation of intestinal PEPT1 protein, might contribute to the progression of renal failure as well as the alteration of drug pharmacokinetics.

renal failure; H^+-coupled peptide transporter; intestine

SMALL PEPTIDES, including di- and tripeptides, are the main products of protein digestion in the gut lumen (2, 13). The absorption of small peptides is mediated by H^+-coupled peptide transporter (PEPT1), which is localized at the brush-border membranes of intestinal epithelial cells. Furthermore, PEPT1 mediates the absorption of a broad range of peptide-like drugs, such as β-lactam antibiotics, the anti-cancer agent bestatin, and angiotensin-converting enzyme (ACE) inhibitors (10, 12, 21). Recently, Gangopadhyay et al. (8) reported that uncontrollable diabetes has a profound effect on the expression of intestinal PEPT1.

In chronic renal failure (CRF), morphological and enzymatic abnormalities have been found in the small intestinal mucosa of patients (7) and model rats at 12 wk after nephrectomy (9). For example, the activities of sucrase and maltase were reduced (9), and the expression of intestinal cytochrome *P*-450 was downregulated in rats at 6 wk after nephrectomy (11). However, the activity of some dipeptidases was significantly but weakly increased or unchanged in the isolated brush-border membranes from the nephrectomized rat intestinal mucosa at 8 wk after surgery (31). It seems plausible to presume that the absorptive function of the mucosa in CRF is disturbed. Recently, the impairment of intestinal P-glycoprotein function was reported in CRF rats (30). In CRF, dietary protein is considered to impair residual renal function, and therefore, patients with CRF are recommended to take a low-protein diet to prevent uremia (25). However, the regulation of intestinal PEPT1 in CRF remains unclear. On the basis of this background, we have hypothesized that the alteration of intestinal PEPT1 has implications not only in the pharmacokinetics of peptide-like drugs but also in the progression of renal failure in patients.

In the present study, we examined the functional and expressional changes of intestinal PEPT1 in 5/6 nephrectomized (5/6 NR) rats and demonstrated the effect of CRF on the intestinal absorptive rates of small peptides and peptide-like drugs. We report in this article that the activity of the intestinal peptide transporter was increased in CRF, which was caused by an upregulation of PEPT1 expression at the protein level.

MATERIALS AND METHODS

Materials. [^{14}C]glycylsarcosine (Gly-Sar; 1.78 GBq/mmol) was obtained from Daiichi Pure Chemicals (Ibaraki, Japan). Ceftibuten was from Shionogi (Osaka, Japan). All other chemicals were of the highest purity available.

Animals and their treatment. Male Wistar albino rats (200–220 g) were nephrectomized as described previously (16, 26). Briefly, the right kidney was removed, and the posterior and anterior apical segmental branches of the left renal artery were individually ligated. Sham-operated (sham) animals were used as controls. After surgery, animals were allowed to recover from anesthesia and surgery in cages, with free access to water and standard rat chow containing 23.6% (wt/wt) of protein.

To examine renal function, we maintained rats in metabolic cages for 24 h before the experiments. The blood urea nitrogen (BUN) was determined using the urease-indophenol method. The levels of creatinine in plasma and urine were determined using the Jaffé reaction. For these measurements, we used assay kits from Wako Pure Chemical Industries (Osaka, Japan). The concentration of urinary albumin was measured using an ELISA kit (NEPHRAT II; Exocell, Philadelphia, PA). The intestinal protease activity in the mucosal homogenate of duodenum, jejunum, or ileum was determined using a protease assay kit (Calbiochem, La Jolla, CA) according to the manufacturer's instructions. Data are expressed as percent activity by using trypsin (10 μg) as a positive control. The animal experiments were performed in accordance with the "Guidelines for Animal Experiments of Kyoto University." All protocols were previously approved by the Animal Research Committee, Graduate School of Medicine, Kyoto University.

Address for reprint requests and other correspondence: K. Inui, Dept. of Pharmacy, Kyoto Univ. Hospital, Sakyo-ku, Kyoto 606-8507, Japan (E-mail: inui@kuhp.kyoto-u.ac.jp).

The costs of publication of this article were defrayed in part by the payment of page charges. The article must therefore be hereby marked "*advertisement*" in accordance with 18 U.S.C. Section 1734 solely to indicate this fact.

Morphological studies. The intestinal segments (duodenum, jejunum, and ileum) were fixed in 10% phosphate-buffered saline and stained with hematoxylin-eosin (HE). These stained sections were evaluated using a light microscope, and villous height and crypt depth of only well-orientated sections were measured with IP Lab Spectrum image analysis software (Signal Analytics, Vienna, VA).

In situ loop technique. We examined [^{14}C]Gly-Sar and ceftibuten transport activity by using the in situ loop technique. A cannula with a polyethylene tube was inserted in the portal vein. A loop was set from the duodenum to ileum, and then [^{14}C]Gly-Sar (29.2 μg/kg) with [^{3}H]inulin (14 μg/kg) or ceftibuten (1.5 mg/kg) was introduced into the loop (1 ml/kg). Blood was withdrawn from the portal vein at designated times, and the plasma was immediately separated from erythrocytes by centrifugation. To determine the concentration of [^{14}C]Gly-Sar, we solubilized plasma samples in 0.5 ml of NCS II tissue solubilizer (Amersham Pharmacia Biotech, Uppsala, Sweden) and determined radioactivity in 5 ml of ACS II scintillation cocktail (Amersham Pharmacia Biotech) using liquid scintillation counting. The plasma concentration of ceftibuten was determined using high-performance liquid chromatography as described previously (14).

Western blot analysis. The rabbit anti-PEPT1 antibody was raised against the 15 COOH-terminal amino acids of rat PEPT1 (21). Goat anti-villin polyclonal IgG was obtained from Santa Cruz Biotechnology (Santa Cruz, CA). While animals were under anesthesia, small intestinal tissue was removed and flushed with cold PBS, and then the mucosa was scraped. A portion of the mucosa was rapidly frozen in liquid nitrogen for the later preparation of crude plasma membrane fractions. Crude plasma membrane fractions were prepared as described previously (18) and were separated by 10% SDS-PAGE and analyzed by immunoblotting with each antibody as reported previously (21). The relative amounts of the bands in each lane were determined densitometrically using NIH Image 1.61 (National Institutes of Health, Bethesda, MD).

Competitive PCR analysis. Competitive PCR was performed according to the method of Siebert and Larrick (22) with some modifications as described previously (16, 26). Briefly, total RNA (1 μg), isolated from rat small intestine using RNeasy mini kit (Qiagen, Hilden, Germany), was reverse transcribed with random hexamers, using Superscript II reverse transcriptase (Invitrogen, Carlsbad, CA), and digested by RNase H (Invitrogen). After a 10-fold dilution of the reaction mixture, 5-μl aliquots were used for subsequent PCR (20 μl). After denaturation of the first-strand DNA at 95°C for 3 min, PCR was performed at 94°C for 1 min, 60°C for 1 min, and 72°C for 1 min for 34 cycles with competitor DNAs (2.5×10^{-19} mol/reaction). Primer sets specific for PEPT1 were as follows: sense primer, 5′-GTGTGGGGCCCCAATCTATACCGT-3′, corresponding to bases 1442–1465, and antisense primer, 5′-GTTTGTCTGTGAGACAGGTTCCAA-3′, corresponding to bases 2153–2176. The expected size of the amplified products derived from the mRNA was 735 bp, and that from the mimic competitor was 607 bp. The amplified PCR products were separated by electrophoresis on 1.7% agarose gels and stained with ethidium bromide. The reactive amounts of bands in each reaction were determined densitometrically using NIH Image 1.61. The densitometric data were normalized for each batch of RNA by correcting the amount of glyceraldehyde-3-phosphate dehydrogenase (GAPDH) mRNA as an internal control.

Measurement of plasma T_3 concentration. The plasma concentration of thyroid hormone 3,5,3′-L-triiodothyronine (T_3) was measured using an enzyme immunoassay method (IMx; Dainabot, Tokyo, Japan).

Statistical analysis. Data were analyzed statistically with the unpaired *t*-test. Probability values $<5\%$ were considered significant.

RESULTS

Renal functional data of 5/6 NR rats. As shown in Table 1, body weight tended to decrease in 5/6 NR rats. The levels of BUN and urinary albumin excretion were significantly increased, and the creatinine clearance was markedly decreased in 5/6 NR rats compared with sham rats. Therefore, the marked renal dysfunction was confirmed. In addition, the progressive renal failure in 5/6 NR rats in the postoperative period was also shown at 4 and 8 wk after nephrectomy.

Morphological studies. Investigators in our laboratory (27) previously reported that tubular damage was minimal at 2 wk after 5/6 NR, although glomerular hypertrophy was observed. We expected little histological alteration in the small intestine at 2 wk after the 5/6 NR. Histological examination of the small intestine in 5/6 NR rats showed no abnormalities at 2 wk after nephrectomy (Fig. 1*A*). We then evaluated the villous height and crypt depth by quantitative analysis. As shown in Fig. 1*B*, both villous height and crypt depth were comparable in sham and 5/6 NR rats. In addition, no abnormality in HE staining, villous height, and crypt depth was found in the 5/6 NR rats at 4 and 8 wk after surgery (data not shown). In addition, we examined the intestinal protease activity by using the trypsin as a positive control. Although the mucosal protease activity tended to be higher in the duodenum than in jejunum or ileum, there was no significant difference between sham and 5/6 NR rats at 2 wk after surgery (Fig. 1*C*).

Gly-Sar and ceftibuten absorption by in situ intestinal loops. We examined the change in intestinal absorption of [^{14}C]Gly-Sar at 2 wk after 5/6 nephrectomy using the in situ intestinal loop technique. Plasma concentration profiles of [^{14}C]Gly-Sar and [^{3}H]inulin in the portal vein after intraintestinal administration are shown in Fig. 2. Although the absorption rate of [^{3}H]inulin did not change throughout the period, the initial absorption rate of [^{14}C]Gly-Sar was markedly increased in the 5/6 NR rats compared with the sham rats. The area under the concentration-time curve ($AUC_{0-9\ min}$) for [^{14}C]Gly-Sar was

Table 1. *Body weight, food intake and renal functional data in sham and 5/6 NR rats*

	2 wk		4 wk		8 wk	
	Sham	5/6 NR	Sham	5/6 NR	Sham	5/6 NR
Body weight, g	278.2±6.3	233.9±5.4*	318.69±6.9	292.1±7.3	381.8±7.6	336.3±11.5
Food intake, g/24 h	21.5±0.6	17.9±0.3*	22.3±0.4	20.2±1.0	ND	ND
BUN, mg/dl	17.9±1.4	55.7±9.2*	17.0±0.9	36.4±4.9*	15.9±0.6	58.7±6.1*
PCr, mg/dl	0.4±0.0	1.0±0.1*	0.4±0.0	1.0±0.1*	0.4±0.0	1.2±0.2*
Ccr, ml·min^{-1}·kg^{-1}	6.9±0.3	2.9±0.2*	7.5±0.5	3.2±0.3*	7.7±0.7	2.7±0.3*
Ualb, mg/24 h	0.3±0.1	4.1±1.2*	0.7±0.2	9.6±2.9*	0.8±0.2	117.7±35.8*

Values are means ± SE of 8–10 rats. BUN, blood urea nitrogen; Pcr, plasma creatinine; Ccr, creatinine clearance; Ualb, urinary albumin excretion; ND, not determined; 5/6 NR, 5/6 nephrectomized. *$P < 0.05$, significantly different from sham rats.

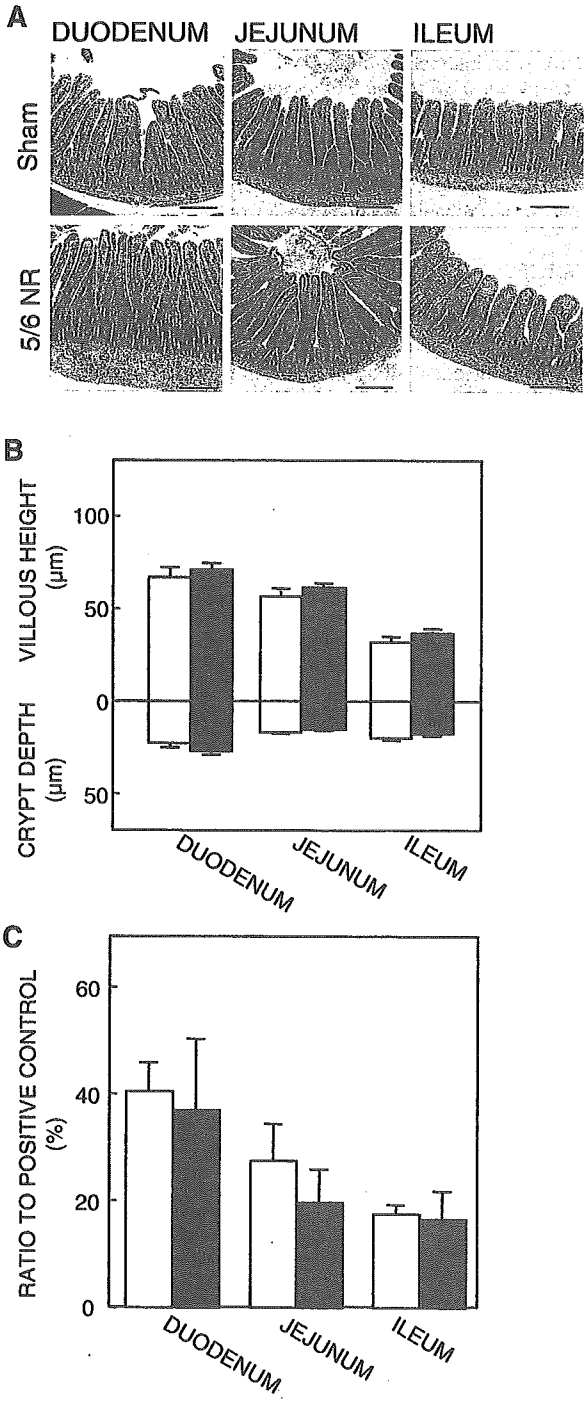

Fig. 1. Histological analysis of intestine in rats after 5/6 nephrectomy (5/6 NR). *A*: small intestinal hematoxylin-eosin staining of sham and 5/6 NR rats at 2 wk after surgery. Magnification, ×40; bar, 20 μm. *B*: small intestinal villous height and crypt depth of sham (open bars) and 5/6 NR rats (filled bars) at 2 wk after surgery. Each value represents the mean ± SE of 8 rats. Six villous height and crypt depth measurements were made for each rat. *C*: mucosal protease activities of sham (open bars) and 5/6 NR rats (filled bars) at 2 wk after surgery. Each value represents the mean ± SE of 5 rats. Data are expressed as percentages of trypsin activity (10 μg) as a positive control.

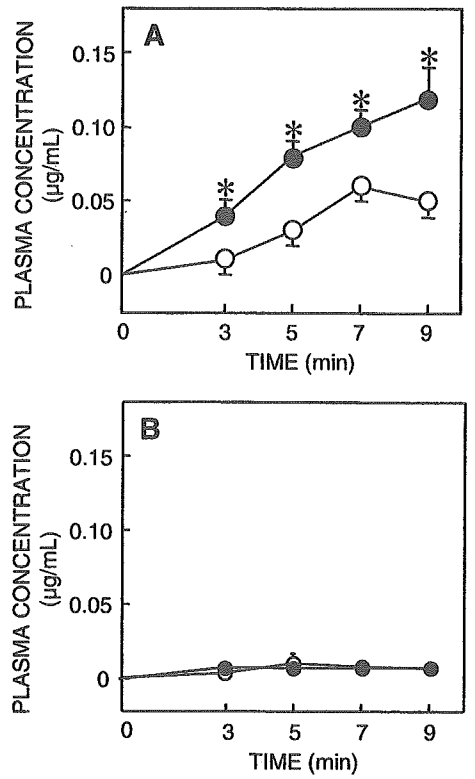

Fig. 2. Plasma concentration of [^{14}C]glycylsarcosine (*A*) and inulin (*B*) in portal vein of sham (○) and 5/6 NR rats (●) after intraintestinal administration, at 2 wk after surgery. Each data point represents the mean ± SE of 6 rats. $*P <$ 0.05, significantly different from sham rats.

0.25 ± 0.06 μg·min·ml^{-1} in sham rats and 0.57 ± 0.05 μg·min·ml^{-1} in 5/6 NR rats (mean ± SE of 6 rats; $P < 0.05$ vs. sham rats) (Fig. 2*A*). Next, the alteration to the absorptive rate of a peptide-like drug, ceftibuten, was examined (Fig. 3). Because ceftibuten was a good substrate of apical PEPT1 but not of basolateral peptide transporter (28), the transcellular transport of ceftibuten was considered to be delayed compared with Gly-Sar. Therefore, the time course of ceftibuten absorp-

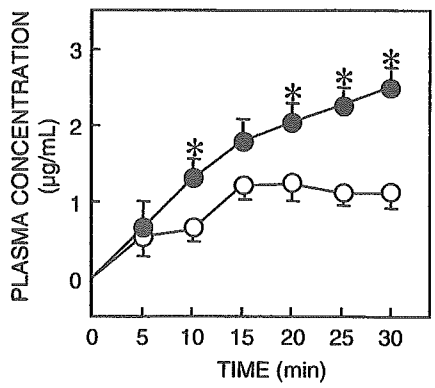

Fig. 3. Plasma concentration of ceftibuten in portal vein of sham (○) and 5/6 NR (●) rats after intraintestinal administration, at 2 wk after surgery. Each data point represents the mean ± SE of 6 rats. $*P < 0.05$, significantly different from sham rats.

tion was set up to 30 min. Similarly, the absorptive rate of ceftibuten also was enhanced in the 5/6 NR rats compared with the sham rats. The $AUC_{0-30\ min}$ for ceftibuten was 26.2 ± 4.5 $\mu g \cdot min \cdot ml^{-1}$ in sham rats and 46.3 ± 6.4 $\mu g \cdot min \cdot ml^{-1}$ in 5/6 NR rats (mean ± SE of 6 rats; $P < 0.05$ vs. sham rats).

Detection of intestinal PEPT1 protein. Western blot analysis was performed to detect the change in the expression level of intestinal PEPT1 protein after 5/6 nephrectomy. At 2 wk after nephrectomy, the expression level of PEPT1 protein in the duodenum was significantly increased in 5/6 NR rats compared with sham rats (Fig. 4). In contrast, in the jejunum and ileum, the expression level of PEPT1 protein in 5/6 NR rats was comparable to that in sham rats. There were no differences in the expression level of villin protein between sham and 5/6 NR rats throughout any segment of the small intestine (Fig. 4).

Detection of intestinal PEPT1 mRNA. To examine the regulation of intestinal PEPT1 mRNA in 5/6 NR rats, we carried out a semiquantitative PCR analysis. The data obtained by competitive PCR were normalized to the data from the competitive PCR for GAPDH. As shown in Fig. 5, the expression level of intestinal PEPT1 mRNA in 5/6 NR rats was not significantly different from that in sham rats at 2 wk after surgery.

Plasma concentration of T_3 in 5/6 NR rats. Investigators in our laboratory (3) previously reported that T_3 treatment downregulated the activity and expression of the intestinal PEPT1. To examine the effect of T_3 with the upregulation of PEPT1 protein in 5/6 NR rats, we measured plasma T_3 concentrations in 5/6 NR rats. As a result, no significant difference was observed in plasma T_3 levels between sham and 5/6 NR rats at 2 wk after surgery (sham, 0.49 ± 0.03 ng/ml vs. 5/6 NR, 0.40 ± 0.05 ng/ml; mean ± SE of 6 rats).

Effect of renal failure progression on expression of intestinal PEPT1 protein. Because the upregulation of intestinal PEPT1 was caused by the protein level, not the mRNA level, the increased level of PEPT1 protein might be a transient phenomenon. Therefore, we have further examined the regulation of intestinal PEPT1 in 5/6 NR rats concerning the time after nephrectomy, i.e., progression of renal impairment. The enterocyte PEPT1 proteins in 5/6 NR rats were detected at 4 and 8 wk after surgery by using Western blot analysis. As shown in Fig. 6, duodenal upregulation of PEPT1 was maintained at 4 and 8 wk after 5/6 nephrectomy. In addition, the expression of PEPT1 in the jejunum was significantly increased in 5/6 NR rats compared with sham rats at 8 wk after surgery. In contrast, the expression level in the ileum was comparable to that in sham rats for at least 8 wk after surgery.

DISCUSSION

Intestinal PEPT1 has physiological and pharmacological roles, such as maintaining protein nutrition and the absorption of peptide-like drugs (6). In addition, two isoforms of peptide transporter (PEPT1 and PEPT2) are expressed in the kidney (10, 12). Recently, investigators in our laboratory (26) found that renal tubular PEPT2, but not PEPT1, was upregulated in 5/6 NR rats. Considering the intestinal localization of PEPT1 and the heightened risk from a protein diet in CRF patients, the functional and molecular regulation of the intestinal PEPT1 should be more important to prevent a protein diet-induced progressive renal failure and/or the adverse effects of peptide-

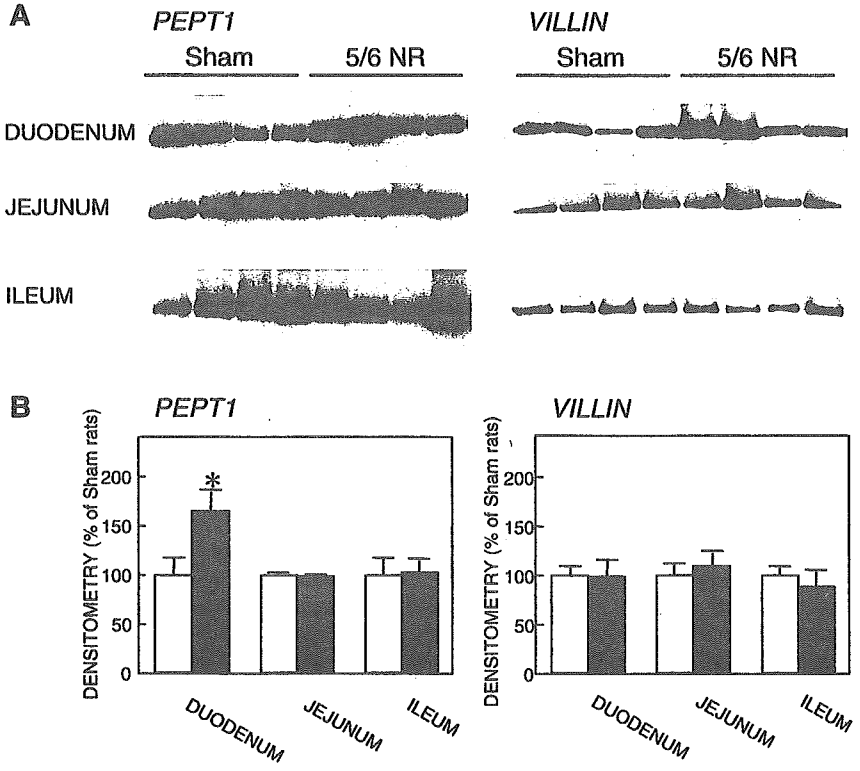

Fig. 4. Western blot analysis of intestinal H^+-coupled peptide transporter (PEPT1) and villin proteins in sham and 5/6 NR rats at 2 wk after surgery. *A*: crude membrane fractions (25 μg) from each intestinal segment were separated by SDS-PAGE (10%) and blotted onto Immobilon P membranes. Antisera specific for PEPT1 and villin (1:1,000 dilution) were used as primary antibodies. Horseradish peroxidase-conjugated anti-rabbit (for PEPT1) or anti-goat (for villin) IgG antibody was used for detection of bound antibodies, and strips of blots were visualized by chemiluminescence on X-ray film. *B*: protein bands are expressed in densitometry units for sham (open bars) and 5/6 NR rats (filled bars). Values for sham rats have been arbitrarily defined as 100%. Each value represents the mean ± SE of 5 rats. *$P < 0.05$, significantly different from sham rats.

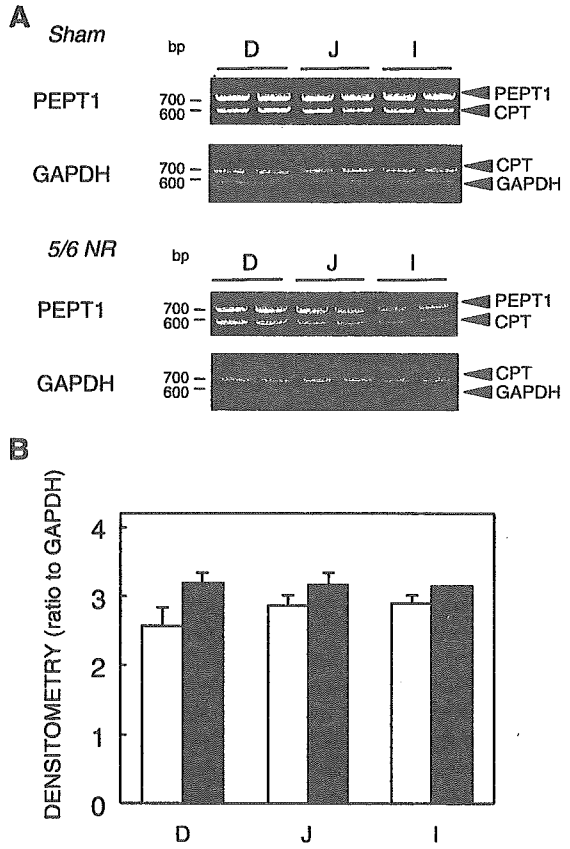

Fig. 5. Detection of PEPT1 and glyceraldehyde-3-dehydrogenase (GAPDH) mRNA in intestinal total RNA isolated from sham and 5/6 NR rats by competitive PCR. *A*: PCR amplification was carried out as described in MATERIALS AND METHODS. Gels show results of representative experiments; arrowheads indicate positions of each protein. CPT, competitor; D, duodenum; J, jejunum; I, ileum. *B*: densitometric determination of PEPT1 mRNA. Data were derived by dividing the ratio between densitometric data for PEPT1 and competitor for PEPT1 by the ratio between densitometric data for GAPDH and competitor for GAPDH, as an internal control. Each value represents the mean ± SE of 5 rats.

like drugs. However, the regulation of intestinal PEPT1 under CRF has not been elucidated. In the present study, we found that the intestinal transport activity of [^{14}C]Gly-Sar and ceftibuten as well as the expression of intestinal PEPT1 protein was upregulated in 5/6 NR rats at 2 wk after surgery (Figs. 2 and 3). Because the expression level of intestinal PEPT1 mRNA in 5/6 NR rats was not significantly different from that in sham rats, this upregulation of PEPT1 by 5/6 nephrectomy was likely caused by a posttranscriptional modification and/or stabilization of the PEPT1 protein. In contrast to the present results, Sterner et al. (23) showed that the small intestinal absorptive capacity of dipeptides was not affected by nephrectomy in rats. This discrepancy may be explained by the difference in the segments of in situ loops used. Whereas Sterner et al. (23) used jejunal segments, we examined the transport activity of dipeptides in the whole small intestine (from duodenum to ileum) (Fig. 2*A*). Because our results show an upregulation of intestinal PEPT1 with 5/6 nephrectomy mainly in the upper region (Figs. 4 and 6), they might have failed to observe this change.

Although morphological abnormalities are found in the small intestine of patients in CRF (7), Haines et al. (9) and Wizemann et al. (31) reported that no significant morphological change was observed in nephrectomized rats comparable with our results. The time span of renal disease in humans is not the same as that in the present animal model. Therefore, a histological evaluation of the small intestine should be made in the future, to confirm the morphological alterations that occurred in 5/6 NR rats at ~20 wk after surgery. In the present study, we examined the intestinal permeability of inulin in 5/6 NR rats and found no significant difference from sham rats (Fig. 2*B*). In addition, no morphological and enzymatic abnormalities were found in the intestinal mucosa of 5/6 NR rats at 2 wk after surgery (Fig. 1). Considering the present results as well as the previous findings (7, 9, 11, 31), the increase of the intestinal PEPT1 may have occurred before other morphological and enzymatic alteration after nephrectomy. These results support the hypothesis that the increase of absorption of [^{14}C]Gly-Sar and ceftibuten in the early phase of CRF was a specific event caused by the upregulation of PEPT1.

Earlier investigations suggested that the activity of PEPT1 varies in response to several factors (1). Dietary proteins are considered as a regulatory factor for intestinal PEPT1. Pan et al. (19) reported that the expression of rat PEPT1 in the duodenum is increased by starvation. In the present study, upregulation of PEPT1 was observed mainly in the upper region of the small intestine of 5/6 NR rats. These results may be partly explained by the reduced food intake in CRF. We monitored the amount of food intake in sham and 5/6 NR rats. The intake was reduced at 2 wk after nephrectomy but recovered to a comparable level with that for sham rats at 4 wk after surgery (Table 1). We found that the expression level of PEPT1 in the duodenum was upregulated in 5/6 NR rats at 4 wk as well as 2 wk after surgery (Fig. 5). Haines et al. (9) also showed that food intake did not significantly differ between nephrectomized and sham rats. Therefore, the variation of food intake after nephrectomy would not relate to the upregulation of PEPT1 protein expression in the small intestine. Other possibilities including hormonal regulation of PEPT1 also have been studied. For example, insulin and leptin stimulated the uptake of dipeptides in human intestinal Caco-2 cells by increasing the translocation of PEPT1 protein from a preformed cytoplasmic pool (5, 29). The treatment of thyroid hormone T_3 and epidermal growth factor (EGF) downregulated the activity and expression of PEPT1 in intestinal cells (3, 17). Moreover, it has been reported that cAMP and protein kinase C activation inhibited the activity of PEPT1 (4, 15). Because the plasma levels of many hormones appear abnormal in CRF (24), we examined the relationship between the plasma T_3 level and the upregulation of PEPT1 protein in 5/6 NR rats. However, we did not find a significant difference in the plasma T_3 level between sham and 5/6 NR rats. In addition, we could not detect the mRNA for gastrointestinal leptin in either rat, and there was no significant difference in the intestinal EGF mRNA level between sham and 5/6 NR rats (data not shown). It was suggested that other factors, including the plasma EGF or insulin level, or other unknown regulators might be related to the upregulation of PEPT1 in CRF. Further studies are required to determine the precise mechanism of upregulation of PEPT1 protein in progressive CRF.

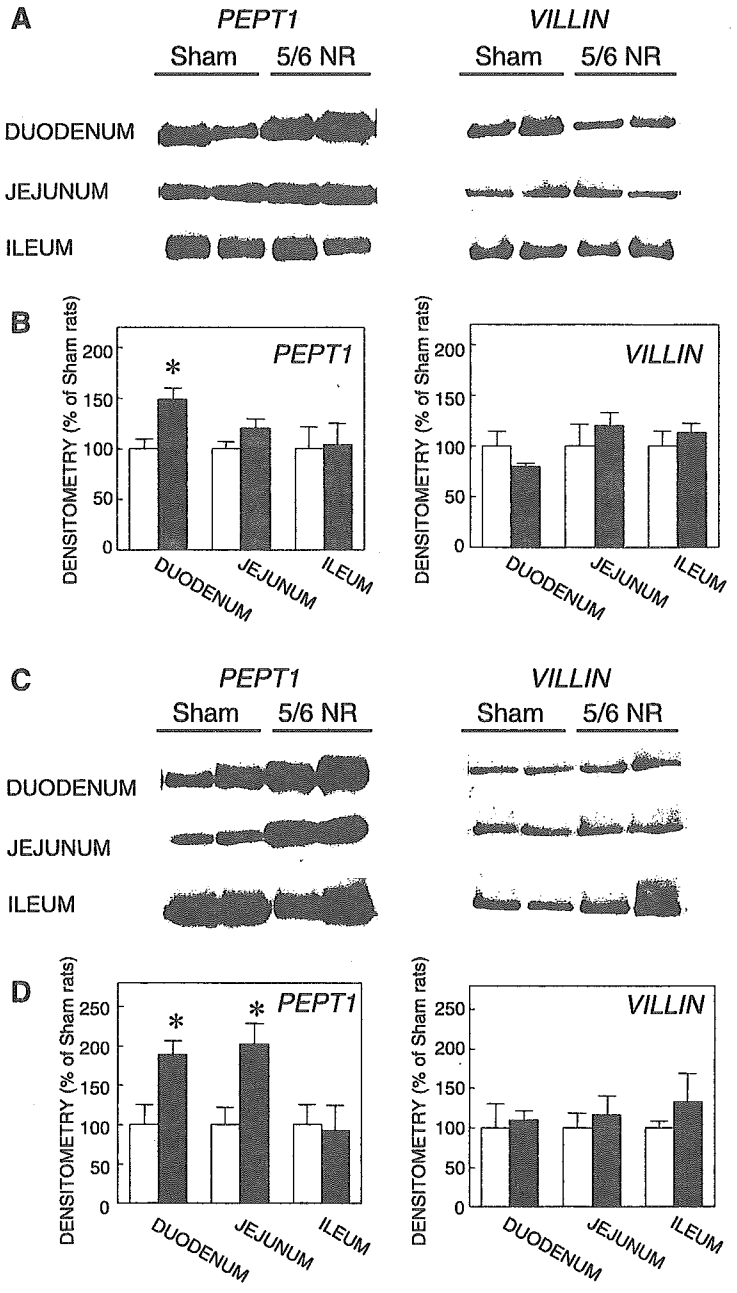

Fig. 6. Western blot analysis of PEPT1 and villin proteins in crude membrane fractions of small intestine isolated from sham and 5/6 NR rats at 4 (*A* and *B*) and 8 wk (*C* and *D*) after surgery. *A* and *C*: blots show results of representative experiments with crude plasma membrane fractions at 4 (*A*) and 8 wk (*C*) after 5/6 NR. *B* and *D*: protein bands are expressed in densitometry units for sham (open bars) and 5/6 NR rats (filled bars). Values for sham rats were arbitrarily defined as 100%. Each value represents the mean ± SE of 5 rats. $^*P < 0.05$, significantly different from sham rats.

In CRF, dietary protein is thought to impair the residual renal function (25). In the present study, we found that the activity of intestinal PEPT1 was upregulated in CRF, accompanied by an increase in the absorption of oligopeptides derived from digested dietary proteins. In addition, we found that the upregulation of intestinal PEPT1 in CRF spread from the upper to lower region with the progression of renal failure (Fig. 6). These results suggest that the upregulation of intestinal PEPT1 and subsequent heightened absorption rate of small peptides relate the escalation in the plasma peptide level and subsequent progressive renal dysfunction. On the other hand, PEPT1 mediates the absorption of peptide-like drugs such as β-lactam antibiotics and ACE inhibitors as well as oligopeptides (10). It is well acknowledged that the urinary excretion rates of these drugs are markedly decreased in CRF. Investigators in our laboratory (27) previously demonstrated that the expression of renal PEPT2, but not PEPT1, was upregulated in CRF and would partly contribute to the delayed urinary excretion rate of peptide-like drugs. In addition to the upregulation of renal PEPT2, the upregulation of intestinal PEPT1 mediated the increased absorption rate of dipeptides and peptide-like drugs. Therefore, the exposure to peptide-like drugs would be prolonged by the sum of the upregulation of intestinal PEPT1 and renal PEPT2 as well as the decreased glomerular filtration

rate in CRF. In patients with hypertension and diabetic nephropathy, ACE inhibitors and angiotensin receptor blockers are used to protect renal function (20). Therefore, a small oral dosage of ACE inhibitors in these patients would provide a sufficient blood level and pharmacological effects to prevent CRF through enhanced absorption via enterocyte PEPT1 and reabsorption via renal PEPT2. Taken together, these data suggest that a careful dosage adjustment according to the intestinal absorptive capacity as well as renal function is needed in patients in CRF.

In the present study, we have demonstrated the upregulation of intestinal PEPT1 expression, which is not regulated by the mRNA level in 5/6 NR rats. The increased expression level of the enterocyte PEPT1 would be a molecular mechanism of accumulation of peptide-like drugs in addition to the decreased glomerular filtration and upregulation of renal PEPT2. In addition, the enhanced absorptive rate or bioavailability of oligopeptides due to the heightened enterocyte PEPT1 expression would partially be a risk factor for the dietary protein-induced progression of CRF. The upregulation of intestinal PEPT1 in 5/6 NR rats was suggested to spread with the progression of renal failure. These results provide useful information for understanding the progressive mechanism of renal failure and for the appropriate usage of peptide-like drugs by considering intestinal function.

GRANTS

This work was supported by a Grant-in-Aid from the Japan Health Sciences Foundation, by a Grant-in-Aid for Scientific Research from the Ministry of Education, Science, Sports, and by the 21st Century Center of Excellence program Knowledge Information Infrastructure for Genome Science.

REFERENCES

1. **Adibi SA.** Regulation of expression of the intestinal oligopeptide transporter (Pept-1) in health and disease. *Am J Physiol Gastrointest Liver Physiol* 285: G779–G788, 2003.
2. **Adibi SA and Mercer DW.** Protein digestion in human intestine as reflected in luminal, mucosal, and plasma amino acid concentrations after meals. *J Clin Invest* 52: 1586–1594, 1973.
3. **Ashida K, Katsura T, Motohashi H, Saito H, and Inui K.** Thyroid hormone regulates the activity and expression of the peptide transporter PEPT1 in Caco-2 cells. *Am J Physiol Gastrointest Liver Physiol* 282: G617–G623, 2002.
4. **Brandsch M, Miyamoto Y, Ganapathy V, and Leibach FH.** Expression and protein kinase C-dependent regulation of peptide/H^+ co-transport system in the Caco-2 human colon carcinoma cell line. *Biochem J* 299: 253–260, 1994.
5. **Buyse M, Berlioz F, Guilmeau S, Tsocas A, Voisin T, Péranzi G, Merlin D, Laburthe M, Lewin MJ, Rozé C, and Bado A.** PepT1-mediated epithelial transport of dipeptides and cephalexin is enhanced by luminal leptin in the small intestine. *J Clin Invest* 108: 1483–1494, 2001.
6. **Daniel H.** Molecular, and integrative physiology of intestinal peptide transport. *Annu Rev Physiol* 66: 361–384, 2004.
7. **Denneberg T, Lindberg T, Berg NO, and Dahlqvist A.** Morphology, dipeptidases and disaccharidases of small intestinal mucosa in chronic renal failure. *Acta Med Scand* 195: 465–470, 1974.
8. **Gangopadhyay A, Thamotharan M, and Adibi SA.** Regulation of oligopeptide transporter (Pept-1) in experimental diabetes. *Am J Physiol Gastrointest Liver Physiol* 283: G133–G138, 2002.
9. **Haines DJ, Swan CH, Green JR, and Woodley JF.** Mucosal peptide hydrolase and brush-border marker enzyme activities in three regions of the small intestine of rats with experimental uraemia. *Clin Sci (Lond)* 79: 663–668, 1990.
10. **Inui K and Terada T.** Dipeptide transporters. In: *Membrane Transporters as Drug Targets,* edited by Amidon GL and Sadée W. New York: Kluwer Academic/Plenum, 1999, p. 269–288.
11. **Leblond FA, Petrucci M, Dubé P, Bernier G, Bonnardeaux A, and Pichette V.** Downregulation of intestinal cytochrome P450 in chronic renal failure. *J Am Soc Nephrol* 13: 1579–1585, 2002.
12. **Leibach FH and Ganapathy V.** Peptide transporters in the intestine and the kidney. *Annu Rev Nutr* 16: 99–119, 1996.
13. **Mathews DM and Adibi SA.** Peptide absorption. *Gastroenterology* 71: 151–161, 1976.
14. **Matsumoto S, Saito H, and Inui K.** Transcellular transport of oral cephalosporins in human intestinal epithelial cells, Caco-2: interaction with dipeptide transport systems in apical and basolateral membranes. *J Pharmacol Exp Ther* 270: 498–504, 1994.
15. **Muller U, Brandsch M, Prasad PD, Fei YJ, Ganapathy V, and Leibach FH.** Inhibition of the H^+/peptide cotransporter in the human intestinal cell line Caco-2 by cyclic AMP. *Biochem Biophys Res Commun* 218: 461–465, 1996.
16. **Nakamura N, Masuda S, Takahashi K, Saito H, Okuda M, and Inui K.** Decreased expression of glucose and peptide transporters in rat remnant kidney. *Drug Metab Pharmacokinet* 19: 41–47, 2004.
17. **Nielsen CU, Amstrup J, Steffansen B, Frokjaer S, and Brodin B.** Epidermal growth factor inhibits glycylsarcosine transport and hPepT1 expression in a human intestinal cell line. *Am J Physiol Gastrointest Liver Physiol* 281: G191–G199, 2001.
18. **Ogihara H, Saito H, Shin BC, Terado T, Takenoshita S, Nagamachi Y, Inui K, and Takata K.** Immuno-localization of H^+/peptide cotransporter in rat digestive tract. *Biochem Biophys Res Commun* 220: 848–852, 1996.
19. **Pan X, Terada T, Okuda M, and Inui K.** Altered diurnal rhythm of intestinal peptide transporter by fasting and its effects on the pharmacokinetics of ceftibuten. *J Pharmacol Exp Ther* 307: 626–632, 2003.
20. **Poulsen PL, Ebbehoj E, Nosadini R, Fioretto P, Deferrari G, Crepaldi G, and Mogensen CE.** Early ACE-i intervention in microalbuminuric patients with type 1 diabetes: effects on albumin excretion, 24 h ambulatory blood pressure, and renal function. *Diabetes Metab* 27: 123–128, 2001.
21. **Saito H, Okuda M, Terada T, Sasaki S, and Inui K.** Cloning and characterization of a rat H^+/peptide cotransporter mediating absorption of beta-lactam antibiotics in the intestine and kidney. *J Pharmacol Exp Ther* 275: 1631–1637, 1995.
22. **Siebert PD and Larrick JW.** Competitive PCR. *Nature* 359: 557–558, 1992.
23. **Sterner G, Lindberg T, and Denneberg T.** In vivo and in vitro absorption of amino acids and dipeptides in the small intestine of uremic rats. *Nephron* 31: 273–276, 1982.
24. **Sweny P, Farrington K, and Moorhead JF.** Chronic renal failure: clinical features and complications. In: *The Kidney and Its Disorders.* London: Blackwell Scientific, 1989, p. 366–374.
25. **Sweny P, Farrington K, and Moorhead JF.** Chronic renal failure: conservative treatment. In: *The Kidney and Its Disorders.* London: Blackwell Scientific, 1989, p. 375–381.
26. **Takahashi K, Masuda S, Nakamura N, Saito H, Futami T, Doi T, and Inui K.** Upregulation of H^+-peptide cotransporter PEPT2 in rat remnant kidney. *Am J Physiol Renal Physiol* 281: F1109–F1116, 2001.
27. **Takahashi K, Nakamura N, Terada T, Okano T, Futami T, Saito H, and Inui K.** Interaction of β-lactam antibiotics with H^+/peptide cotransporters in rat renal brush-border membranes. *J Pharmacol Exp Ther* 286: 1037–1042, 1998.
28. **Terada T, Sawada K, Saito H, Hashimoto Y, and Inui K.** Functional characteristics of basolateral peptide transporter in the human intestinal cell line Caco-2. *Am J Physiol Gastrointest Liver Physiol* 276: G1435–G1441, 1999.
29. **Thamotharan M, Bawani SZ, Zhou X, and Adibi SA.** Hormonal regulation of oligopeptide transporter Pept-1 in a human intestinal cell line. *Am J Physiol Cell Physiol* 276: C821–C826, 1999.
30. **Veau C, Leroy C, Banide H, Auchère D, Tardivel S, Farinotti R, and Lacour B.** Effect of chronic renal failure on the expression and function of rat intestinal P-glycoprotein in drug excretion. *Nephrol Dial Transplant* 16: 1607–1614, 2001.
31. **Wizemann V, Ludwig D, Kuhl R, and Burgmann I.** Digestive-absorptive function of the intestinal brush border in uremia. *Am J Clin Nutr* 31: 1642–1646, 1978.

Computational modelling of H$^+$-coupled peptide transport via human PEPT1

Megumi Irie[1], Tomohiro Terada[1], Toshiya Katsura[1], Satoshi Matsuoka[2] and Ken-ichi Inui[1]

[1]*Department of Pharmacy, Kyoto University Hospital, Faculty of Medicine, Kyoto University, Kyoto 606-8507, Japan*
[2]*Department of Physiology and Biophysics, Kyoto University Graduate School of Medicine, Kyoto 606-8501, Japan*

H$^+$-coupled peptide transporter 1 (PEPT1) mediates the transport of small peptides and peptide-like drugs in a pH- and voltage-dependent manner. Here, we investigated the transport mechanisms of PEPT1 for neutral and charged substrates by experimental studies and computational simulation. Uptake studies revealed that the Michaelis-Menten constant (K_m) of glycylsarcosine (Gly-Sar), a neutral substrate, decreased with a fall in pH from 7.4 to 5.5, but at pH 5.0, the K_m increased again. In contrast, the K_m value of an anionic substrate, ceftibuten, declined steadily with decreasing pH. Based on these findings and information from the literature, we hypothesized the transport mechanisms in which (1) H$^+$ binds to not only the H$^+$-binding site, but also the substrate-binding site; and (2) H$^+$ at the substrate-binding site inhibits the interaction of neutral and cationic substrates, but is necessary for that of anionic substrates. To validate these hypotheses, a computational model was constructed and various properties of substrate transport by PEPT1 were simulated. Our model reproduced the voltage dependence, hyperbolic saturation and bell-shaped pH-profile of Gly-Sar transport. Moreover, the various transport properties of negatively and positively charged substrates were also reconstructed. These findings indicated that the inferred mechanisms are able to sufficiently interpret the transport of both neutral and charged substrates by PEPT1.

(Received 5 February 2005; accepted after revision 24 March 2005; first published online 31 March 2005)
Corresponding author K. Inui: Department of Pharmacy, Kyoto University Hospital, Sakyo-ku, Kyoto 606-8507, Japan. Email: inui@kuhp.kyoto-u.ac.jp

H$^+$-coupled peptide transporter 1 (PEPT1) expressed in the brush-border membranes of intestinal epithelial cells mediates the transport of small peptides from the lumen into the cells, and therefore plays an important role in the absorption of protein (Leibach & Ganapathy, 1996; Adibi, 1997; Terada & Inui, 2004). In addition, because of its broad substrate specificity, PEPT1 can accept various pharmacologically active compounds, including β-lactam antibiotics, and serve as an absorptive pathway for these drugs (Inui & Terada, 1999; Daniel & Kottra, 2004; Terada & Inui, 2004). Numerous functional studies have demonstrated that PEPT1 utilizes the H$^+$ electrochemical gradient as a driving force and exhibits an obvious pH dependence, and that transport by PEPT1 is electrogenic and voltage-dependent regardless of the net charge of the substrate (Fei *et al.* 1994; Mackenzie *et al.* 1996*a*; Daniel, 2004).

Although the transport characteristics have been delineated, the fundamental transport mechanisms of PEPT1 remain unclear. For example, in the uptake of most neutral substrates, including the typical substrate glycylsarcosine (Gly-Sar), a bell-shaped pH profile with maximal activity at pH 5.5–6.0 is commonly observed (Fei *et al.* 1994; Steel *et al.* 1997; Terada *et al.* 1999), but it has not been elucidated why the uptake of these substrates is reduced under more acidic conditions such as at pH 5.0, despite an increase in the H$^+$ gradient. In addition, the pH profiles of differently charged substrates are distinct from those of neutral substrates (Matsumoto *et al.* 1994; Mackenzie *et al.* 1996*a*; Wenzel *et al.* 1996; Amasheh *et al.* 1997; Steel *et al.* 1997), the cause of which has not been clarified. Furthermore, it is still controversial how PEPT1 handles differently charged substrates with H$^+$, including the stoichiometry (Daniel, 2004; Terada & Inui, 2004).

Previously, based on electrophysiological studies, Mackenzie *et al.* (1996*b*) proposed a kinetic model of Gly-Sar transport by PEPT1. Using the partial reactions of this model, the properties of the pre-steady-state currents induced by PEPT1 in the absence of substrate were well represented (Mackenzie *et al.* 1996*b*). However, it has not been demonstrated whether the model of Mackenzie *et al.* (1996*b*) can also display the various features of the steady-state currents evoked by Gly-Sar transport via PEPT1. Furthermore, their model was proposed for Gly-Sar transport only, and therefore it is unclear whether the model can be applied to charged substrates.

DOI: 10.1113/jphysiol.2005.084582

Table 1. Equations for the computational simulation of PEPT1 function

$$P(C_o) = \frac{1}{\left\{1 + \left(\frac{[Sc]_o}{K_{d,Soc1}}\right) + \left(\frac{[H]_o}{K_{d,Ho}}\right)\left(1 + \frac{[Sc]_o}{K_{d,Soc2}} + \frac{[Sn]_o}{K_{d,Son}}\right) + \left(\frac{[H]_{os}}{K_{d,Hos}}\right)\left(\frac{[H]_o}{K_{d,Ho}}\right)\left(1 + \frac{[Sa]_o}{K_{d,Soa}}\right)\right\}} \quad (1)$$

$$P(C_oS_c) = \frac{1}{\left\{1+\left(\frac{K_{d,Soc1}}{[Sc]_o}\right)\left[1+\left(\frac{[H]_o}{K_{d,Ho}}\right)\left[1+\frac{[Sc]_o}{K_{d,Soc2}}+\frac{[Sn]_o}{K_{d,Son}}+\left(\frac{[H]_{os}}{K_{d,Hos}}\right)\left(1+\frac{[Sa]_o}{K_{d,Soa}}\right)\right]\right]\right\}} \quad (2)$$

$$P(C_oHS_c) = \frac{1}{\left\{1+\left(\frac{K_{d,Soc2}}{[Sc]_o}\right)\left[1+\frac{[Sn]_o}{K_{d,Son}}+\left(\frac{K_{d,Ho}}{[H]_o}\right)\left(1+\frac{[Sn]_o}{K_{d,Soc1}}\right)+\left(\frac{[H]_{os}}{K_{d,Hos}}\right)\left(1+\frac{[Sa]_o}{K_{d,Soa}}\right)\right]\right\}} \quad (3)$$

$$P(C_oHS_n) = \frac{1}{\left\{1+\left(\frac{K_{d,Son}}{[Sn]_o}\right)\left[1+\frac{[Sc]_o}{K_{d,Soc2}}+\left(\frac{K_{d,Ho}}{[H]_o}\right)\left(1+\frac{[Sc]_o}{K_{d,Soc1}}\right)+\left(\frac{[H]_{os}}{K_{d,Hos}}\right)\left(1+\frac{[Sa]_o}{K_{d,Soa}}\right)\right]\right\}} \quad (4)$$

$$P(C_oHHS_a) = \frac{1}{\left\{1+\left(\frac{K_{d,Soa}}{[Sa]_o}\right)\left[1+\left(\frac{K_{d,Hos}}{[H]_{os}}\right)\left[1+\frac{[Sn]_o}{K_{d,Son}}+\frac{[Sc]_o}{K_{d,Soc2}}+\left(\frac{K_{d,Ho}}{[H]_o}\right)\left(1+\frac{[Sc]_o}{K_{d,Soc1}}\right)\right]\right]\right\}} \quad (5)$$

$$a = k_1 \cdot P(C_o) + k_3 \cdot P(C_oS_c) + k_5 \cdot P(C_oHS_c) + k_7 \cdot P(C_oHS_n) + k_9 \cdot P(C_oHHS_a) \quad (6)$$

$$b = k_2 \cdot P(C_i) + k_4 \cdot P(C_iS_c) + k_6 \cdot P(C_iHS_c) + k_8 \cdot P(C_iHS_n) + k_{10} \cdot P(C_iHHS_a) \quad (7)$$

$$\text{fluxS} = N\left\{\begin{array}{l} y\left[k_3 \cdot P(C_oS_c) + k_5 \cdot P(C_oHS_c) + k_7 \cdot P(C_oHS_n) + k_9 \cdot P(C_oHHS_a)\right] \\ -(1-y)\left[k_4 \cdot P(C_iS_c) + k_6 \cdot P(C_iHS_c) + k_8 \cdot P(C_iHS_n) + k_{10} \cdot P(C_iHHS_a)\right] \end{array}\right\} \quad (8)$$

$$\text{fluxH} = N\left\{\begin{array}{l} y\left[k_5 \cdot P(C_oHS_c) + k_7 \cdot P(C_oHS_n) + 2k_9 \cdot P(C_oHHS_a)\right] \\ -(1-y)\left[k_6 \cdot P(C_iHS_c) + k_8 \cdot P(C_iHS_n) + 2k_{10} \cdot P(C_iHHS_a)\right] \end{array}\right\} \quad (9)$$

$$k_x = k_x \exp(-z\gamma VF/2/R/T) \quad (10)$$

$$k_x = k_x \exp(z\gamma VF/2/R/T) \quad (11)$$

$$[X]_{eff} = [X]_{sol} \exp(-z\alpha FV/R/T) \quad (12)$$

$$I_{PEPT1} = \sum \text{flux}/F/z \quad (13)$$

The equations used for the simulation of the functional properties of PEPT1 are summarized. Five equations (eqns (1–5)) for calculation of the probabilities (*P*) were derived from the 14-state model shown in Fig. 3*A*. The representations in the equations and the procedure of simulation using these equations are described in Methods. *P*(X), the probability of the state X; [X], the concentration of X; C, carrier (PEPT1); H, proton; S, substrate; K_dX, the dissociation constant of X; k_x, the rate constants; the subscripts a, n and c, the charge of substrate (a, anion; n, neutral; c, cation); the subscripts o and i, the facing direction of PEPT1 (o, facing the extracellular side; i, facing the intracellular side).

In the present study, to reveal the transport mechanisms of PEPT1, we first examined the effects of pH on the transport of Gly-Sar and ceftibuten, an oral anionic β-lactam antibiotic, in detail. Based on our experimental results and the previous studies, we hypothesized the transport mechanisms in which (1) H^+ binds not only to the H^+-binding site, but also to the substrate-binding site; and (2) H^+ at the substrate-binding site inhibits the interaction of neutral and cationic substrates, but is necessary for that of anionic substrates. Furthermore, to validate the hypothesized mechanisms, we constructed a computational model, and the transport of neutral and charged substrates by PEPT1 was simulated.

Methods

Cell culture and uptake studies

Caco-2 cells (American Type Culture Collection CRL-1392) were cultured on 12-well cluster plates or 35 mm plastic dishes as previously described (Irie *et al.* 2001), and used on the 14th or 15th day for experiments between passages 33 and 45. Uptake studies using [^{3}H]Gly-Sar (PerkinElmer) and ceftibuten (gift from Shionogi) were performed as previously reported (Matsumoto *et al.* 1994; Terada *et al.* 1999).

Computational modelling of PEPT1

The simulation program was created using Visual Basic.NET. Based on the presumed recognition patterns of PEPT1 for neutral and charged substrates (Fig. 2), we constructed a 14-state model (Fig. 3*A*). We assumed that H^+ and peptide bindings to PEPT1 are rapid and instantaneously equilibrated. Transitions between PEPT1 facing the extracellular and intracellular sides, denoted as 'o' and 'i', respectively, in Fig. 3*A* and the equations (Table 1), are reduced to a two-state reaction as described in the Na^+–K^+ pump model (Matsuoka *et al.* 2003). PEPT1 faces the extracellular side in the seven states: empty state (C_o), cationic substrate-bound state (C_oS_c), H^+ and cationic substrate-bound state (C_oHS_c), H^+ and neutral substrate-bound state (C_oHS_n), one H^+-bound state (C_oH), two H^+-bound state (C_oHH), and two H^+ and anionic substrate-bound state (C_oHHS_a). The probabilities (*P*) of C_o, C_oS_c, C_oHS_c, C_oHS_n, and C_oHHS_a are calculated using eqns (1–5) (Table 1) where *P*(X) stands for the probability of state X, [X] for the 'effective concentration' of X as described below, and $K_{d,S}$ and $K_{d,H}$ for the dissociation constants of substrates and H^+, respectively. The subscripts c, n and a stand for cationic, neutral and anionic charges of substrates, respectively. $K_{d,Soc1}$ and $K_{d,Soc2}$ are the dissociation constants of

cationic substrates for PEPT1 without or with H^+ at the H^+-binding site, respectively. Because of little information about the efflux properties of PEPT1, we assumed the same mechanism for the intracellular side, and the probabilities of the states facing the interior side were calculated in a similar way as the eqns (1–5) (Table 1). When the 14-state model was condensed into a two-state model (Fig. 3*B*), the rate constants (a, b) were calculated using the eqns (6) and (7) (Table 1), and then the net fluxes of substrate (fluxS) or H^+ (fluxH) in the time unit were calculated with the probabilities and rate constants (k_{1-10}) using the eqns (8) and (9) (Table 1), in which N stands for the number of PEPT1 proteins.

We assumed that transporters in states C_o and C_i bear one negative charge, and those in C_oHS_n and C_iHS_n are neutral. For S_c carrying one positive charge, we considered that the transporters in C_oHS_c and C_iHS_c have one positive charge, and those in C_oS_c and C_iS_c are neutral. If S_c is a dication, the transporters in C_oHS_c and C_iHS_c bear two positive charges, whereas those in C_oS_c and C_iS_c are monovalent. When S_a has one or two negative charges, we assumed the transporters in C_oHHS_a and C_iHHS_a are neutral and carry one negative charge, respectively. The rate constants (k_{1-10}) were defined based on the Eyring theory of reaction rates (Parent *et al.* 1992*b*; Mackenzie *et al.* 1996*b*) as described by the eqns (10) and (11) (Table 1), in which $\tilde{k}_x$ stands for the voltage-independent value of k_x, z($= -1, 0, +1$ or $+2$ in this study) for the net charge which moves with each transmembrane transition, and γ ($= 0.73$) for the fractional dielectric distance. F, V, R and T in the equations have their usual meanings. k_1, k_3, k_5, k_7 and k_9 are described by eqn (10) (Table 1), and k_2, k_4, k_6, k_8 and k_{10} by eqn (11) (Table 1).

The concentrations of ionic species of substrate ($[X]_{sol}$) were obtained using the Henderson-Hasselbalch equation with pK_a values. According to Mackenzie *et al.* (1996*b*), we assumed a voltage-dependent binding of H^+ and substrate to the outside of PEPT1 ('ion well'). The 'effective concentrations' of charged species and H^+ ($[X]_{eff}$) at the extracellular binding site, the bottom of the 'well', were calculated using eqn (12) (Table 1) (Matsuoka *et al.* 2003). For simplicity, we assumed the same fractional distance for the H^+-binding site and the substrate-binding site. Concerning the fractional distance, $\alpha + \gamma = 1$. For the simulation of electrophysiological studies, the current generated by PEPT1 (I_{PEPT1}) was calculated using the Faraday constant and the net charges which move with transmembrane transition by eqn (13) (Table 1).

Simulation

The steady-state fraction of y in the reduced two-state model was obtained as $y = b/(a + b)$. For the simulation of pre-steady-state currents in the absence of substrate, the differential equation was solved using Euler's method with a time step of 0.05 ms. We obtained almost the same result with a time step of 0.005 ms. The concentrations of ionic species of substrate at different pH values were calculated using pK_a values. In all simulations, the intracellular pH was defined as 7.4.

Results

Studies regarding pH dependence of Gly-Sar and ceftibuten uptake

The pH dependence of 20 μM Gly-Sar transport by PEPT1 exhibited a bell-shaped curve (Fig. 1*A*). As shown in Fig. 1*B*, more than 91% of Gly-Sar is neutral at a pH of 5.0–7.4, indicating that the bell-shaped pH profile is attributable to the function of PEPT1, and not to the change in the charge of Gly-Sar. Next, the kinetic parameters (K_m and V_{max}) of Gly-Sar for PEPT1 at various pH values were estimated. The V_{max} value gradually increased as the pH dropped from 7.4 to 5.0, whereas the K_m value decreased markedly with a fall in the pH to 5.5, and when the pH reached 5.0, increased again (Fig. 1*C*). Previous studies suggested that the coupling ratio of a neutral substrate to H^+ is 1:1, and that the binding of H^+ occurs prior to that of substrate (Fei *et al.* 1994; Mackenzie *et al.* 1996*b*). According to this, the increase in K_m at alkaline pH is expected, because the proportion of protonated PEPT1 is small and much substrate is necessary to shift the equilibrium of the state of PEPT1 from that having H^+ only to that in which both H^+ and substrate reside. However, this theory cannot explain the increase in K_m at pH 5.0.

For the increase in K_m at acidic pH, we hypothesized that H^+ competes with Gly-Sar at the substrate-binding site, and elevates the K_m value and reduces the uptake. However, this assumption does not apply to anionic substrates such as ceftibuten, because the pH profiles of some anionic substrates do not exhibit a reduction at acidic pH (Matsumoto *et al.* 1994; Wenzel *et al.* 1996). Thus, concerning anionic substrates, we formulated two hypotheses: (1) in contrast to Gly-Sar, the binding of H^+ to the substrate-binding site is necessary for the binding of substrates bearing a negative charge, and therefore competitive inhibition does not occur; (2) besides H^+ at the H^+-binding site, H^+ at the substrate-binding site is cotransported with anionic substrates. These hypotheses were based on previous studies which demonstrated that the transport of negatively charged substrates by PEPT1 evoked inward currents (Mackenzie *et al.* 1996*a*; Wenzel *et al.* 1996; Steel *et al.* 1997), and that the intracellular acidification accompanied by the transport of anionic substrates was more rapid than that accompanied by the transport of neutral substrates (Steel *et al.* 1997; Kottra *et al.* 2002).

To examine these hypotheses, pH dependence of ceftibuten uptake was investigated. As shown in Fig. 1*D*, the uptake increased sharply as the pH dropped. Within the range of pH used, the principal ionic species was mono- or dianion (Fig. 1*E*), demonstrating that PEPT1 can transport substrates carrying a net negative charge. Moreover, the K_m value of ceftibuten decreased along with the pH, and no increase was observed at the lower pH (Fig. 1*F*). These findings are consistent with the hypotheses stated above.

Construction of transport model for PEPT1

By integrating the findings of the present and previous studies, we constructed a novel model for the transport of H^+ and substrate via PEPT1. Figure 2 is the scheme for the recognition patterns of PEPT1 in terms of charges of substrates. We defined that all substrates share the same substrate-binding site because substrate transport by PEPT1 obeys the Michaelis-Menten equation, and exhibits the competitive inhibition among substrates irrespective

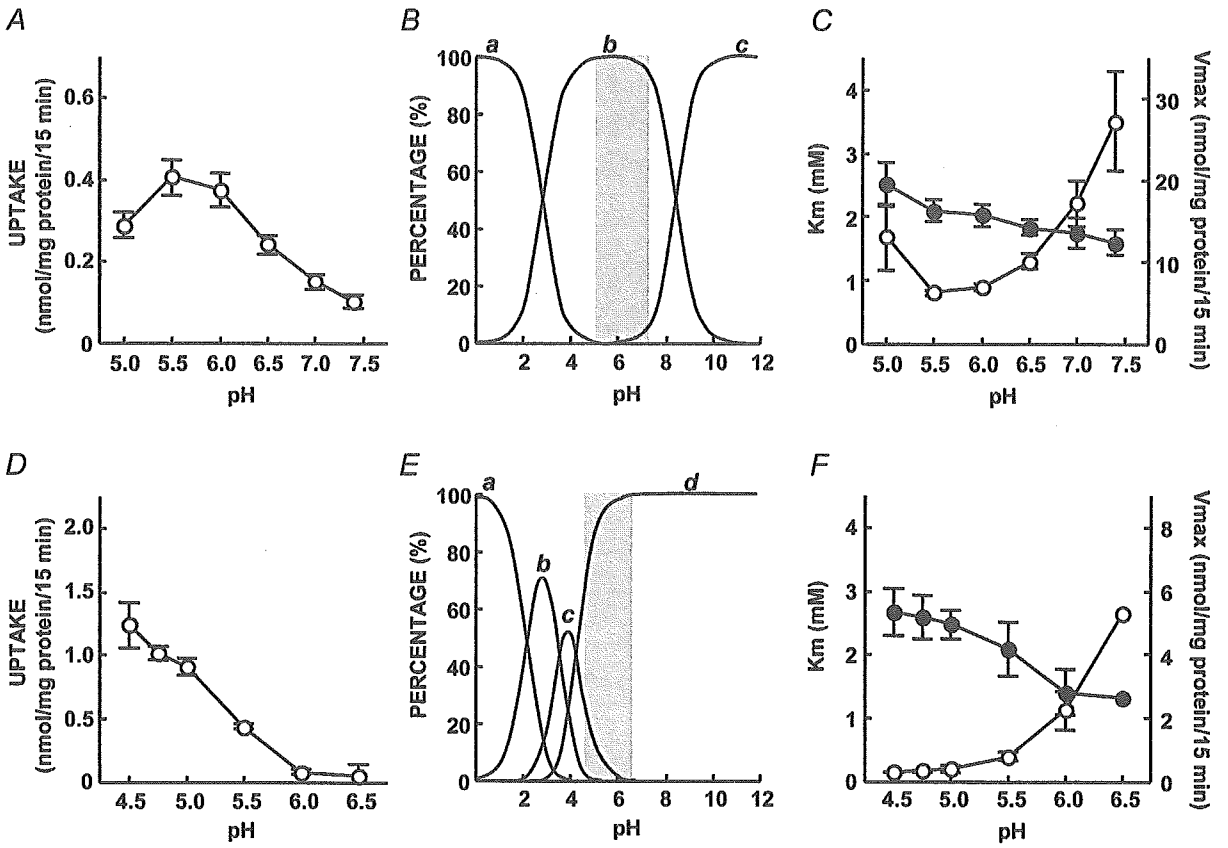

Figure 1. Effects of pH on the charge or uptake of Gly-Sar or ceftibuten
A, pH dependence of [^{3}H]Gly-Sar uptake by PEPT1. The uptake of 20 μM [^{3}H]Gly-Sar from the apical side in Caco-2 cells was measured at various pH values (37°C). Each symbol represents the specific uptake calculated by subtracting the nonspecific uptake from total uptake. The nonspecific uptake was estimated by multiplication of the substrate concentration (20 μM) and the K_d value obtained by the experiments on concentration dependence. *B*, the percentage of ionic species of Gly-Sar as a function of pH. The percentages of monocationic (*a*), neutral (*b*) and monoanionic (c) species of Gly-Sar were calculated using the pK_a values (pK_{a1} = 2.83, pK_{a2} = 8.45) by the Henderson-Hasselbalch equation. *C*, pH dependence of the kinetic parameters of [^{3}H]Gly-Sar uptake by PEPT1. The uptake of [^{3}H]Gly-Sar at various concentrations (20–10 000 μM) and pH values (pH 5.0–7.4) was measured at 37°C, and K_m (○) and V_{max} (●) values were estimated using Michaelis-Menten equation. *D*, pH dependence of ceftibuten uptake by PEPT1. The uptake of 50 μM ceftibuten from the apical side in Caco-2 cells was measured at pH 4.5–6.5 by HPLC, and the specific uptake was calculated to be similar to [^{3}H]Gly-Sar. *E*, the percentage of ionic species of ceftibuten as a function of pH. The percentages of monocationic (*a*), neutral (*b*), monoanionic (c) and dianionic (*d*) species of ceftibuten were calculated using the pK_a values (pK_{a1} = 2.17, pK_{a2} = 3.67, pK_{a3} = 4.07). *F*, pH dependence of the kinetic parameters of ceftibuten uptake. The uptake of ceftibuten at various concentrations (50–10000 μM) and pH values (pH 4.5–6.5) was measured and K_m (○) and V_{max} (●) values were estimated. *A* and *D*, each symbol represents the mean ± S.E.M. of nine independent monolayers from three separate experiments. *B* and *E*, the shadowed zone represents the range of pH used for the uptake studies. *C* and *F*, the symbols show the means ± S.E.M. of three independent experiments.

of charges (Wenzel *et al.* 1996; Sawada *et al.* 1999), and that empty PEPT1 has one negative charge (Mackenzie *et al.* 1996*b*). It was also defined that PEPT1 has one H^+-binding site to which H^+ is bound prior to substrate, except for the case of cationic substrates (described below). At high pH, as most PEPT1 proteins do not have H^+ at the H^+-binding site (Fig. 2, left), neutral and anionic substrates could not interact. However, we did not exclude the possibility that cationic substrates can interact with empty PEPT1 and be transported without H^+, considering that the intracellular acidification as a consequence of the transport of cationic substrates was moderate (Steel *et al.* 1997; Kottra *et al.* 2002). At moderate pH values, as most PEPT1 proteins have H^+ at the H^+-binding site, both cationic and neutral substrates can be recognized and transported (Fig. 2, middle). As described above, it was assumed that anionic substrates cannot access the substrate-binding site lacking H^+, and that the protonated substrate-binding site can accept only negatively charged substrates (Fig. 2, right). Based on the above hypotheses, a kinetic model for the transport mechanism of PEPT1 was constructed (Fig. 3*A*). To avoid an increase in the number of unknown parameters, the model was made as simple as possible. Next, various simulations were performed to validate this model.

Simulation of the transport of Gly-Sar and ceftibuten

The parameters used for the simulation were described in the legend of Fig. 3, where the values for $\tilde{k}_1$, $\tilde{k}_2$, α and γ were cited from Mackenzie *et al.* (1996*b*). With these four values fixed, other parameters were determined so as to fit the data of Gly-Sar transport (Mackenzie *et al.* 1996*b*). Although other parameter values may be possible, the set of parameters used in this study could reproduce global observations as shown in Figs 4–6, indicating adequacy. In all simulations, the intracellular concentration of substrate was defined as 0, thus the dissociation constants of substrates at the interior binding site were not determined in this study.

Figure 4 shows the simulation for the electrophysiological studies by Mackenzie *et al.* (1996*b*). The time profiles of the transient charge movements induced by various voltage steps in the absence of substrate were well simulated (Fig. 4*A*), suggesting that our model can quantitatively represent pre-steady-state properties of PEPT1. Furthermore, our model reproduced the inward currents accompanied by Gly-Sar transport, the current–voltage relationship at various concentrations of Gly-Sar (Fig. 4*B*), and voltage dependence of K_m values for Gly-Sar (Fig. 4*C*) and for H^+ (not shown). We then simulated Gly-Sar uptake by Caco-2 cells using a membrane potential fixed at −57 mV, a value that was obtained experimentally (Grasset *et al.* 1984). The saturable uptake conforming to the Michaelis-Menten mode (Fig. 5*A*), the bell-shaped pH profiles (Fig. 5*B*) and the alteration in K_m value by pH (Fig. 5*C*) fitted the experimental data. These findings indicate that the voltage dependence, the concentration dependence and the pH dependence of Gly-Sar transport by PEPT1 can be interpreted by our model.

Next, ceftibuten uptake in Caco-2 cells was simulated using parameters identical to those used for the simulation above, except for the dissociation constants of substrates. As shown in Fig. 5*D–F*, the hyperbolic saturation, pH profiles of the uptake and pH dependence of the kinetic parameters corresponded to the observations, indicating that our model can be applied to anionic substrates.

Simulation of the transport of various charged substrates

Finally, in addition to Gly-Sar, various transport properties of PEPT1 were simulated for charged substrates, anionic

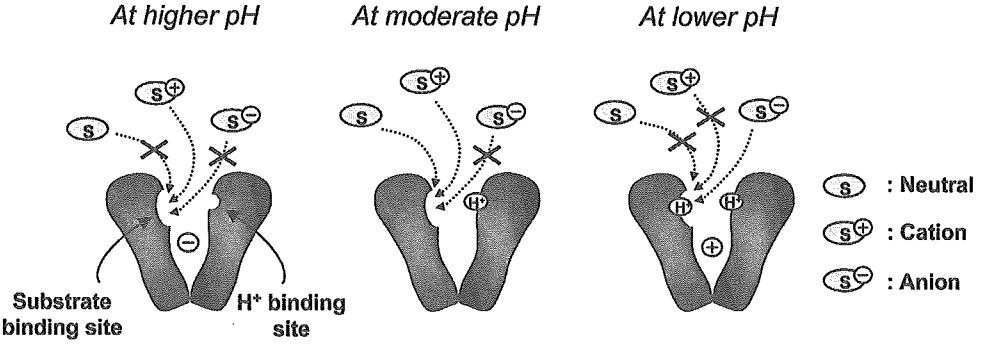

Figure 2. Scheme for the recognition patterns of PEPT1 for neutral and charged substrates
Left, neither neutral substrates nor anionic ones can be recognized by empty PEPT1, which is the principle state at higher pH. Empty PEPT1 can accept only cationic substrates. Middle, at moderate pH, H^+ binds to H^+-binding site, and PEPT1 with H^+ on the H^+-binding site can recognize neutral and cationic substrates, but not anionic ones. Right, anionic substrates can be accepted by only a protonated substrate-binding site at lower pH.

dipeptide Ala-Asp and cationic dipeptides Ala-Lys and Lys-Gly. As shown in Fig. 6*A* and *B*, the inward currents were induced by anionic, neutral and cationic dipeptides over a broad range of membrane potentials, and the K_m value for the cationic dipeptide Lys-Gly exhibited voltage dependence, corresponding to previous reports (Mackenzie *et al.* 1996*a*; Kottra *et al.* 2002). Figure 6*C* shows the simulated pH profiles for Ala-Asp, Ala-Lys and Lys-Gly. Although proper experimental data for Lys-Gly were not obtained, the simulations of the other dipeptides were similar to the observations (Mackenzie *et al.* 1996*a*). Moreover, the transport ratio of H^+/substrate and the ratio of the total currents induced by the substrate transport to the charge movements by H^+ flux were calculated (Fig. 6*D*). In contrast to both ratios for Gly-Sar of 1, Ala-Asp was cotransported with more than one H^+, but the induced current was less than that expected from H^+ flux. On the other hand, the coupling ratio of Lys-Gly to H^+ was smaller than 1, and the total current evoked by Lys-Gly was larger.

Discussion

Compared with other symporters, such as Na^+/glucose cotransporter 1 (Parent *et al.* 1992*a*,*b*), Na^+/P_i cotransporter 2 (Forster *et al.* 1998) and Na^+/I^- symporter (Eskandari *et al.* 1997), the transport mechanism of PEPT1 has not been clarified. Based on a functional characterization, several studies have proposed the idea for the transport mechanisms of PEPT1 (Mackenzie *et al.* 1996*a*,*b*; Steel *et al.* 1997; Kottra *et al.* 2002), but it has never been examined whether the suggested mechanisms actually describe the transport features of PEPT1. In addition, there is no suggestion for a mechanism which can describe a bell-shaped pH profile of substrate transport via PEPT1. In the present study, by integrating experimental findings with information from the literature, we proposed novel transport mechanisms of PEPT1 applicable to neutral and charged substrates. Furthermore, by computational modelling, we demonstrated that the inferred mechanisms represent global functional features of PEPT1.

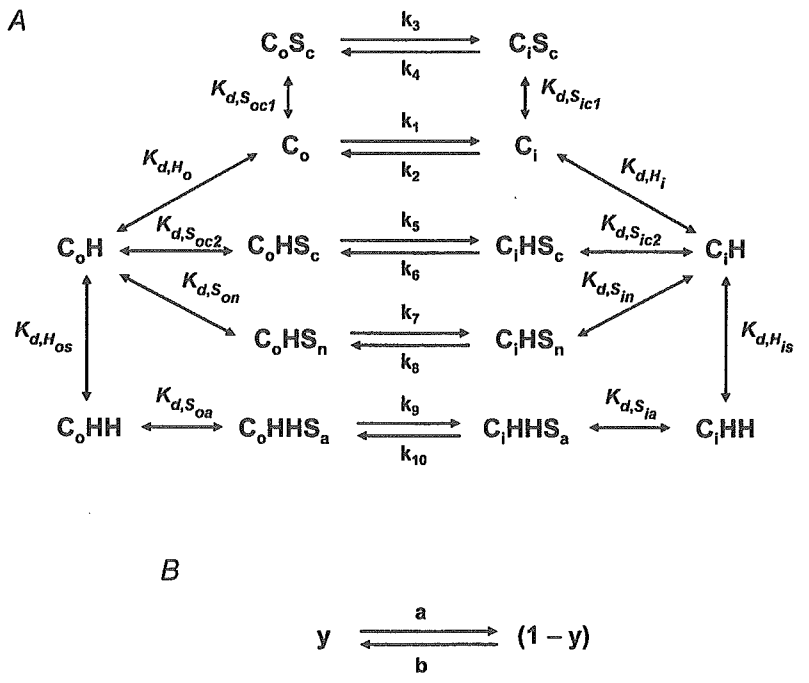

Figure 3. Kinetic transport model of PEPT1
A, the 14-state model for PEPT1. The assumed transport mechanism is represented by a 14-state model as described in Methods. C_o and C_i represent empty PEPT1 facing the exterior and interior sides, respectively, and C_oX and C_iX stand for PEPT1 carrying X. S and H are substrate and H^+, respectively. $K_{d,X}$ represents the dissociation constant of X, and $K_{d,Ho}$ and $K_{d,Hos}$ stand for the dissociation constants of H^+ to the H^+- and substrate-binding sites, respectively. The subscripts a, n and c stand for anionic, neutral and cationic charges of substrates, respectively. The rate constants (k_{1-10}) were calculated using the equations described in the Methods with the following values (per millisecond): $k_1 = 0.32$, $k_2 = 0.082$, $k_3 = 0.6$, $k_4 = 0.6$, $k_5 = 0.02$, $k_6 = 0.02$, $k_7 = 0.6$, $k_8 = 0.6$, $k_9 = 0.2$, $k_{10} = 0.2$. The values of k_1 and k_2 were cited from Mackenzie *et al.* (1996*b*). The dissociation constants of H^+ (μM) and fractional distance are as follows: $K_{d,Ho} = 0.45$, $K_{d,Hos} = 17$, $K_{d,Hi} = 0.45$, $K_{d,His} = 17$, $\alpha = 0.27$, $\gamma = 0.73$. These parameters are common to all substrates simulated. *B*, the reduced two-state model for PEPT1. The 14-state model was condensed into a two-state model, which was used for simulation.

pH profiles of substrate transport via PEPT1

The most important mechanism proposed in this study is the binding of H^+ to the substrate-binding site, which is the essential feature different from all previous suggestions Mackenzie *et al.* 1996*a*,*b*; Steel *et al.* 1997; Kottra *et al.* 2002) and provides a possible solution for various pH profiles observed in the transport of substrates with different charges by PEPT1. According to our model, H^+ at the substrate-binding site competitively inhibits the binding of neutral substrates and results in an increase of K_m and a decrease of uptake at acidic pH. On the other hand, as the binding of H^+ to the H^+-binding site shifts the equilibrium from C_o to C_oH, which can accept neutral substrates (Fig. 3*A*), H^+ exerts an inductive effect on Gly-Sar transport. Therefore, the bell-shaped pH profile is the sum of both inductive and inhibitory effects of H^+ on Gly-Sar transport, i.e. the stimulation is predominant at high pH, but at low pH, the H^+-binding site approaches saturation and the excess H^+ occupies the substrate-binding site, and thus the inhibitory effect of H^+ is elicited.

In contrast to neutral substrates, we suggest that H^+ at the substrate-binding site enables negatively charged substrates to interact with PEPT1. As ceftibuten bears a net negative charge at the pH values used (Fig. 1*E*), H^+ does not inhibit but enhances ceftibuten uptake, and the stimulation of uptake with falling pH was more intensive than that of Gly-Sar because of the inductive effects by two H^+ on both binding sites. In the case of cationic substrates, the effects of H^+ on the substrate transport seem to be more complicated, because the pH profiles of cationic substrates are of variety (Mackenzie *et al.* 1996*a*; Amasheh *et al.* 1997; Guo *et al.* 1999; Kottra *et al.* 2002). Therefore, we hypothesized two mechanisms for the transport of cationic substrates in this model. First, the transport of cationic substrate is affected by H^+ in terms of both induction and inhibition, similar to the case of a neutral substrate (k_5 and k_6 in Fig. 3*A*). Second, the transport of cationic substrate without H^+ is assumed (k_3 and k_4 in Fig. 3*A*), which is inhibited by H^+ on the H^+-binding site because the probability of empty PEPT1 is decreased. Therefore, the effects of H^+ on the transport of cationic substrates are altered by the degree of contribution of two transition steps.

In Fig. 6*C*, pH profiles of both anionic and cationic dipeptides with maximal activity at different pH were shown, which accounted for the mixed effects of various factors, such as the proportion of the ionic charges of substrates, the balances among the dissociation constants of H^+ and substrates. These findings indicate that our model can be applied to differently charged substrates and that the factors described above may be the principal causes determining an apparent pH profile of substrate transport by PEPT1. However, previous studies suggested that the location of charge in the substrate molecule affects the properties of substrate transport (Kottra *et al.* 2002), but

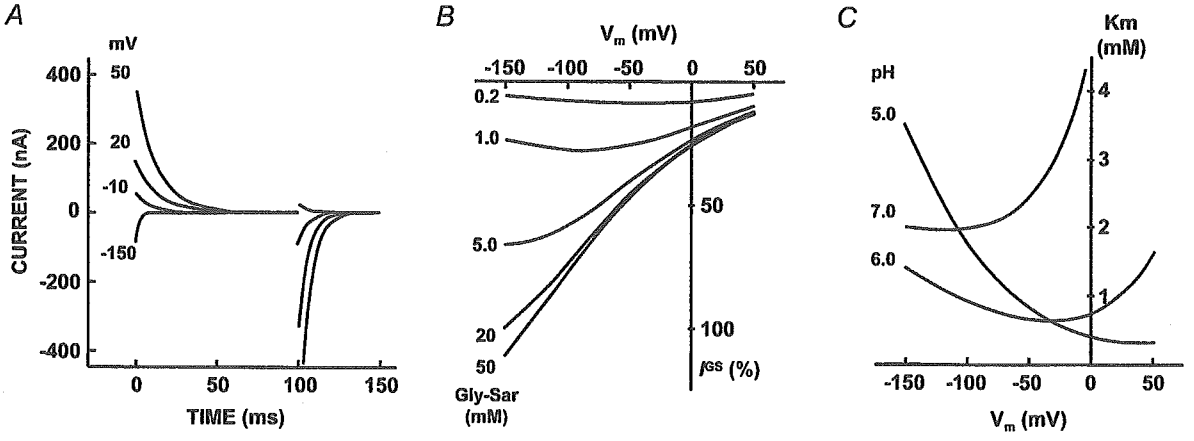

Figure 4. Simulation of electrophysiological properties of PEPT1
A, time profiles of pre-steady state currents by PEPT1. Pre-steady-state currents by PEPT1 in the absence of substrate were simulated using voltage steps from the holding potential (−50 mV) to the indicated potential (−150, −10, 20 or 50 mV) for 100 ms, followed by return of voltage to the holding potential for 50 ms. PEPT1 carrier density and the temperature were assumed as 0.11 pmol per oocyte and 22°C, respectively. *B*, voltage dependence of Gly-Sar-induced currents via PEPT1. Currents evoked by Gly-Sar at various concentrations (0.2–50 mM) were simulated every 0.5 mV under the condition of 22°C, pH 5.0. The magnitude of currents was normalized by that of 20 mM Gly-Sar at −150 mV. *C*, voltage dependence of K_m values of Gly-Sar for PEPT1. Voltage dependence of K_m value for Gly-Sar was simulated. To obtain K_m values, the following calculations were repeated at a membrane voltage of −150 to +50 mV every 0.5 mV at pH 5.0, 6.0 and 7.0. The current of 50 mM Gly-Sar was assumed as I_{max}, and then currents were calculated with increasing concentrations of Gly-Sar from 2 μM with 2 μM increments. The concentration of Gly-Sar that led the current of 50% I_{max} was considered the K_m value. Four dissociation constants of Gly-Sar on the extracellular side ($K_{d,Soc1}$, $K_{d,Soc2}$, $K_{d,Son}$ and $K_{d,Soa}$ in Fig. 3*A*) are defined as 2000 μM.